Decoherence in models for hard-core bosons coupled to optical phonons

A. Dey, M. Q. Lone, and S. Yarlagadda
CMP Div., 1/AF Salt Lake, Saha Institute of Nuclear physics, Kolkata, India 700064
(Received 18 December 2014; published 2 September 2015)

Understanding coherent dynamics of excitons, spins, or hard-core bosons (HCBs) has tremendous scientific and technological implications for quantum computation. Here, we study decay of excited-state population and decoherence in two models for HCBs, namely, a two-site HCB model with site-dependent strong potentials and subject to non-Markovian dynamics and an infinite-range HCB model governed by Markovian dynamics. Both models are investigated in the regimes of antiadiabaticity and strong HCB-phonon coupling with each site providing a different local optical phonon environment; furthermore, the HCB systems in both models are taken to be initially uncorrelated with the environment in the polaronic frame of reference. In the case of the two-site HCB model, we show clearly that the degree of decoherence and decay of excited state are enhanced by the proximity of the site-energy difference to the eigenenergy of phonons and are most pronounced when the site-energy difference is at resonance with twice the polaronic energy; additionally, the decoherence and the decay effects are reduced when the strength of HCB-phonon coupling is increased. For the infinite-range model, when the site energies are the same, we derive an effective many-body Hamiltonian that commutes with the long-range system Hamiltonian and thus has the same set of eigenstates; consequently, a quantum-master-equation approach shows that the quantum states of the system do not decohere.

DOI: 10.1103/PhysRevB.92.094302 PACS number(s): 71.38.−k, 03.65.Yz, 85.35.Be, 87.10.Hk

I. INTRODUCTION

Quantum information processing heavily relies on a precious and fragile resource, namely, quantum entanglement [1]. The fragility of entanglement is due to the coupling between a quantum system and its environment; such a coupling leads to decoherence, the process by which information is degraded. Decoherence is the fundamental mechanism by which fragile superposition of states is destroyed, thereby producing a quantum to classical transition [2,3]. Since coupling of a quantum system to the environment and the concomitant entanglement fragility are ubiquitous [1,2], it is imperative that progress be made in minimizing decoherence.

Modeling and controlling the environment of a solid-state quantum bit is a major challenge in quantum computation. Fairly long coherence times have been achieved in semiconductor-based double-quantum-dot (DQD) systems where the qubit information is encoded in the singlet-triplet states of two spins with total S^z equal to zero [4]. Recently, an oxide-based DQD system [with one electron or hard-core boson (HCB) tunneling between the two identical dots] was proposed as a qubit [5]. This DQD system has the following advantages: (a) similar to semiconductor DQDs [4], oxide-based DQDs permit fast electrical control of the exchange interaction; (b) the extent of the electronic wave function in oxides is an order of magnitude smaller than that in semiconductors and thus oxides are better suited for miniaturization; and (c) the decoherence due to the environment (i.e., optical phonons) in oxide dots is significantly smaller than the decoherence due to the bath of nuclear spins in semiconductor dots.

In general, a many-qubit (i.e., many-particle) system can have distance-dependent interaction. The two limiting cases for interaction are particle (HCB) hopping strength that is independent of distance and a system with nearest-neighbor hopping only. In a quantum computer architecture involving many qubits, it is highly desirable to be able to perform gate operations between any (i.e., nearby or distant) pair of qubits. In this work, we consider an extreme model involving distance-independent interaction of HCBs which can be mapped onto the following spin model: $\sum_{i,j>i}[-J_\perp(S_i^x S_j^x + S_i^y S_j^y) + J_\parallel S_i^z S_j^z]$. Such a model has relevance to many realistic physical systems of interest.

First, the well-studied Lipkin-Meshkov-Glick (LMG) model [6] $H_{\rm LMG} = -2h(\sum_j S_j^z) - 2\lambda[(\sum_j S_j^x)^2 + \gamma(\sum_j S_j^y)^2]/N$ (for $h = 0$ and $\gamma = 1$) is a special case of the above-mentioned long-range model (for $J_\parallel = 0$ and $J_\perp = \lambda$); while, for $h = 0$ and $\gamma = 0$, LMG model is a special case of the model for $J_\perp = 0$ and $J_\parallel = -\lambda$. Long-range interactions between spins or qubits can be produced in cavity quantum electrodynamics as shown by experiments using a quantized cavity mode [7,8]. Using such experiments as inspiration, by varying the external model parameters, it has been proposed that positive and negative values of λ with $\gamma = 1$ can be achieved [9,10]. Furthermore, it has been pointed out in Refs. [8,11] that having the same site energy for the spins and qubits makes the qubit-qubit interaction effective as it conserves energy in the spin flip-flop process; here, the qubit-qubit interaction is mediated by exchange of virtual photons. Second, fully connected network (FCN) is a well-studied model in the context of highly efficient coherent energy transfer processes in light-harvesting complexes [12–14]. FCN is characterized by uniform hopping strength between any pair of sites and is an extreme limit of long-range interaction model for excitons, spins, or HCBs. Moreover, the phonon fluctuations at various sites are uncorrelated to each other [14], i.e., local phonon effects are significant in such complexes. Third, it has been shown by Ezawa that the long-range ferromagnetic Heisenberg model describes well a zigzag graphene nanodisk [15]. Lastly, a two-spin system and a four-spin system (with spins at the corners of a regular tetrahedron) can be physically realized (for instance from a Hubbard model) as exact special cases of the long-range model; it is conceivable that slightly larger

 ©2015 American Physical Society

clusters of particles (for instance, clusters containing six or eight particles) can be physically realized as reasonable approximations of such a model.

In this work, in the regimes of strong HCB-phonon interaction and antiadiabaticity, we consider two HCB models which are generalizations of a two-spin system studied earlier [5]. It was shown in Ref. [5] that a pair of interacting spins, coupled to an optical phonon environment, undergoes small decoherence when both the spins have the same site energies. Here, in the first model, we analyze the case where just one HCB is hopping between two sites with different site energies and the HCB-phonon coupling is local. Using non-Markovian second-order quantum master equation, we find that decoherence as well as decay of the population of the excited state are sizable if the site-energy difference is sufficiently close to the phonon eigenenergies; these features are manifested for both single-mode and multimode optical phonons. The non-Markovian dynamics became relevant because, when the site-energy difference approaches a phonon eigenenergy, the largest effective interaction energy for HCB system is not much smaller than the optical phonon frequency; consequently, the time scale over which the state of the HCB system changes appreciably is not much larger than the correlation time for the environmental fluctuations.

As regards our second HCB model, without specifically modeling cavity QED systems or photosynthetic complexes, we draw inspiration from these systems and identify important features that will produce coherent transport of HCBs in artificial infinite-range, many-site systems. We analyze the nature of decoherence and decay of excited-state population in an infinite-range interaction model for HCBs that are coupled to local optical phonons. In this many-site model, for simplicity, all the sites are taken to be at the same energy; then, the HCB-HCB interaction can be made effective/sizeable using a single cavity mode [8,11]. We show that the effective Hamiltonian in second-order perturbation theory retains the same eigenstates as the infinite-range system Hamiltonian. Our dynamical analysis shows that the system, when Markov processes are considered, neither decoheres nor allows decay of excited states. Such a Markovian approximation is valid for sufficiently small values of the small parameter; such small values are attainable at large electron-phonon couplings and strong antiadiabaticities.

Although a weak interaction permits a Migdal type of perturbative treatment, a strong HCB-phonon interaction requires a nonperturbative approach (involving a phonon vacuum instability) [16]. We study the above-mentioned two HCB models in the polaronic frame of reference where initially the system and the environment constitute a simply separable state. Preparation of such a simply separable initial state has been explicitly described in Sec. VIII of Ref. [5]. In the transformed polaronic frame, the interaction term is weak and enables use of perturbation theory; furthermore, both preparation and measurement can be done in the dressed (polaronic) basis [5,17].

In related studies involving evolution of a charge carrier in the Holstein model that is initially excited and uncoupled to the lattice in the original laboratory frame [18,19], analysis has been carried at weak and strong electron-phonon couplings and in the adiabatic and antiadiabatic regimes. At large antiadiabaticity and for both weak and strong electron-phonon couplings, it was found that there is negligible energy transfer between electron and phonons and that dynamics is governed by coherent oscillations with the frequency of oscillations being the phonon frequency. In the adiabatic regime and at weak coupling, the electron dissipates its energy and enters the stationary regime without fluctuations [18]. As regards the system at strong coupling and strong adiabaticity, initial coherent oscillations are quickly dephased, resulting in a state with excited polarons coexisting with metastable delocalized states [19].

The rest of the paper is organized as follows. In Sec. II, we study decoherence and decay of excited state using a non-Markovian analysis for a system of two sites (each with a different site energy) and single-mode optical phonons. In Sec. III, we introduce the infinite-range HCB Hamiltonian strongly coupled to local optical phonons and derive the effective Hamiltonian. Next, using the master-equation approach, we study decoherence under Markovian dynamics. Finally, in Sec. IV, we give our conclusions and make some general remarks regarding the wider context of our results. The paper also has two Appendixes: the first Appendix deals with multimode phonons for the two-site case involving different site energies; the second Appendix analyzes the small parameter for the two-site system.

II. A SINGLE-MODE, TWO-SITE CASE WITH DIFFERENT SITE ENERGIES

Here, we consider the case where one HCB is hopping between two sites whose site-energy difference is comparable to the phonon eigenenergies; this is in contrast to the case of equal site energies (considered in Ref. [5]) which resulted in negligible decoherence and decay of excited state. We assume that each site has its local phonon environment. Initially, for simplicity, we consider the baths and the interaction terms to involve only a single mode and ignore the wave-number dependence (for an analysis of the multimode case, see Appendix A). The model Hamiltonian is given by

$$\begin{aligned} H = {} & \varepsilon_1\left(n_1-\frac{1}{2}\right)+\varepsilon_2\left(n_2-\frac{1}{2}\right)-\frac{J_\perp}{2}(b_1^\dagger b_2+b_2^\dagger b_1) \\ & + J_\parallel\left(n_1-\frac{1}{2}\right)\left(n_2-\frac{1}{2}\right)+g\omega\sum_{i=1,2}\left(n_i-\frac{1}{2}\right)(a_i+a_i^\dagger) \\ & +\omega\sum_{i=1,2}a_i^\dagger a_i, \end{aligned} \tag{1}$$

where ε_1 and ε_2 are the site energies, $\frac{J_\perp}{2}(>0)$ is the hopping, and $J_\parallel(>0)$ is the repulsion strength between HCBs on the adjacent sites. HCB creation and destruction operators are defined as $b_i^\dagger$ and b_i with the commutation relations given by

$$\begin{aligned} & [b_i,b_j]=[b_i,b_j^\dagger]=0 \quad \text{for } i\neq j, \\ & \{b_i,b_i^\dagger\}=1, \end{aligned} \tag{2}$$

and $n_i \equiv b_i^\dagger b_i$. Furthermore, a_j and $a_j^\dagger$ are the destruction and creation operators of phonons at the jth site, respectively, g is the HCB-phonon coupling constant, and ω is the phonon frequency for the simple harmonic oscillators.

In the regime of strong electron-phonon coupling, we perform the well-known Lang-Firsov (LF) transformation [16,20]

$$H^L \equiv e^S H e^{-S} = H_s^L + H_I^L + H_B^L, \tag{3}$$

where $S = -\sum_i g(n_i - \frac{1}{2})(a_i - a_i^\dagger)$; the operators b_j and a_j transform like fermions and bosons, respectively. The LF transformation produces composite HCBs (involving HCBs clothed with phonons) and displaces the simple harmonic oscillators. We make our analysis in the polaronic frame of reference where the system Hamiltonian H_s^L, interaction Hamiltonian H_I^L, and the displaced-phonon Hamiltonian H_B^L are given by

$$H_s^L = \varepsilon_1\left(n_1 - \frac{1}{2}\right) + \varepsilon_2\left(n_2 - \frac{1}{2}\right) - \frac{J_\perp e^{-g^2}}{2}(b_1^\dagger b_2 + b_2^\dagger b_1) + J_\parallel\left(n_1 - \frac{1}{2}\right)\left(n_2 - \frac{1}{2}\right), \tag{4}$$

$$H_I^L = -\frac{1}{2}[J_\perp^+ b_1^\dagger b_2 + J_\perp^- b_2^\dagger b_1], \tag{5}$$

and

$$H_{\rm env}^L = \omega \sum_{i=1,2} a_i^\dagger a_i, \tag{6}$$

respectively. In the above equations

$$J_\perp^\pm = J_\perp e^{\pm g[(a_2 - a_2^\dagger) - (a_1 - a_1^\dagger)]} - J_\perp e^{-g^2} \tag{7}$$

and

$$J_\perp e^{-g^2} = {}_{ph}\langle 0|J_\perp e^{\pm g[(a_2 - a_2^\dagger) - (a_1 - a_1^\dagger)]}|0\rangle_{ph}. \tag{8}$$

Additionally, $J_\perp^\pm / J_\perp$ is the deviation of the local phonon field from its ground-state expectation value, and thus the ground-state average of this vanishes. The system Hamiltonian H_s^L represents HCB coupled to the mean-phonon field and $\frac{1}{2}J_\perp e^{-g^2}$ is the resulting renormalized hopping amplitude. In the subspace involving only one HCB and two sites, the two eigenstates of H_s^L are given by $\frac{1}{\sqrt{1+\chi_1^2}}(\chi_1|10\rangle + |01\rangle)$ and $\frac{1}{\sqrt{1+\chi_2^2}}(\chi_2|10\rangle + |01\rangle)$ with corresponding eigenenergies $\frac{-J_\parallel - 2\sqrt{\Delta\varepsilon^2 + J_\perp^2 e^{-2g^2}}}{4}$ and $\frac{-J_\parallel + 2\sqrt{\Delta\varepsilon^2 + J_\perp^2 e^{-2g^2}}}{4}$, respectively; here, $\chi_1 = -\frac{\Delta\varepsilon - \sqrt{\Delta\varepsilon^2 + J_\perp^2 e^{-2g^2}}}{J_\perp e^{-g^2}}$ and $\chi_2 = -\frac{\Delta\varepsilon + \sqrt{\Delta\varepsilon^2 + J_\perp^2 e^{-2g^2}}}{J_\perp e^{-g^2}}$ with site-energy difference $\Delta\varepsilon = \varepsilon_1 - \varepsilon_2$. The interaction Hamiltonian H_I^L represents the HCBs coupled to fluctuations of local phonons around their mean-phonon field. Here, in the strong HCB-phonon coupling regime, we want to maintain quantum coherence in the dressed (polaronic) basis; the local-phonon fluctuation, involving large number of uncontrolled degrees of freedom, is the source of noise to the coherent dynamics of the polarons. As the interaction in the polaronic frame of reference is weak (compared to that in the original frame of reference), one can treat H_I^L as a perturbation.

When the site-energy difference approaches the eigenenergy of phonons, the small parameter value becomes sizable, the time scale for the HCB system to change appreciably becomes comparable to the correlation time of the bath fluctuations, and non-Markovian dynamics becomes relevant. In Appendix B, we will discuss the validity of our perturbation theory and the nature of dynamics for the case of unequal site energies.

A. Non-Markovian dynamics of the model

The dynamics of the system, described by the reduced density matrix $\rho_s(t)$ at time t, is obtained from the total system-environment density matrix $\rho_T(t)$ by taking the partial trace over the degrees of freedom of the environment:

$$\rho_s(t) = {\rm Tr}_R[\rho_T(t)]. \tag{9}$$

To analyze the non-Markovian dynamics of the model, in the polaronic frame of reference, we start with the simply separable initial state $\rho_T(0) = \rho_s(0) \otimes R_0$ where $\rho_s(0)$ need not correspond to only the ground state and R_0 is the phonon density matrix at thermal equilibrium and is given by $R_0 = \sum_{n_1,n_2} |n_1,n_2\rangle_{ph\ ph}\langle n_1,n_2| e^{-\beta\omega_{n_1,n_2}}/Z$. Here, n_1 and n_2 are the phonon occupation numbers at sites 1 and 2, respectively; in this section, we will use the notation $|n\rangle_{ph} \equiv |n_1,n_2\rangle_{ph}$ and $\omega_n \equiv \omega_{n_1,n_2} = \omega(n_1 + n_2)$. The preparation of such an initially factorized state was demonstrated in detail (by using a significantly small value of $J_\perp/\omega$) for a realistic system, i.e., an oxide-based double quantum dot (DQD), in Ref. [5]; the effect of fluctuations (given by H_I^L) was shown to be negligible. There, upon realizing the desired initially separable state, the desired value of the tunneling $J_\perp$ could be obtained by changing the gate voltage much faster than the electron can tunnel. Once $J_\perp$ is sizable, fluctuations become relevant and lead to decoherence. Here too, the same procedure can be adopted to obtain the simply separable initial state in a DQD; subsequently, the desired values of detuning ($\Delta\varepsilon$) and tunneling ($J_\perp$) can be achieved by adjusting the relevant voltages much faster than the electron can tunnel across.

Now, although the initial state is simply separable in the polaronic frame, it is given by $e^{-S}\rho_s(0) \otimes R_0 e^S$ in the original frame of reference and is thus an entangled state. Furthermore, as pointed out in Sec. VIII of Ref. [5], the readout can be obtained (noninvasively) in the polaronic frame. *Thus, since the states can be prepared and measured in the dressed (polaronic) basis, we study decoherence as well as decay of the population of the excited state in the polaronic frame and demonstrate below that they are both small when the initial state is simply separable and when the site-energy difference is sufficiently different from the phonon eigenenergies.*

Now, we start with the second-order, time-convolutionless (TCL), non-Markovian, quantum-master equation [i.e., Redfield equation (see Ref. [21])]

$$\frac{d\tilde{\rho}_s(t)}{dt} = -\int_0^t d\tau\, {\rm Tr}_R\big[\tilde{H}_I^L(t), \big[\tilde{H}_I^L(\tau), \tilde{\rho}_s(t) \otimes R_0\big]\big], \tag{10}$$

where $\tilde{H}_I^L(t) = e^{iH_0^L t} H_I^L e^{-iH_0^L t}$ and $\tilde{\rho}_s(t) = e^{iH_0^L t}\rho_s(t)e^{-iH_0^L t}$ are the interaction Hamiltonian and the reduced density matrix operators (respectively) expressed in the interaction picture; $H_0^L = H_s^L + H_{\rm env}^L$ is the unperturbed Hamiltonian. Furthermore, in the above Eq. (10), it has been assumed that ${\rm Tr}_R[\tilde{H}_I^L(t), \rho_s(0) \otimes R_0] = 0$ which is certainly valid at temperature 0 K. Next, at zero temperature, Eq. (10) can be

rewritten as

$$\frac{d\tilde{\rho}_s(t)}{dt} = -\sum_m \int_0^t d\tau \Big[{}_{ph}\langle 0|\tilde{H}_I^L(t)|m\rangle_{ph}\ {}_{ph}\langle m|\tilde{H}_I^L(\tau)|0\rangle_{ph}\tilde{\rho}_s(t) - {}_{ph}\langle m|\tilde{H}_I^L(t)|0\rangle_{ph}\tilde{\rho}_s(t)_{ph}\langle 0|\tilde{H}_I^L(\tau)|m\rangle_{ph}$$
$$- {}_{ph}\langle m|\tilde{H}_I^L(\tau)|0\rangle_{ph}\tilde{\rho}_s(t)_{ph}\langle 0|\tilde{H}_I^L(t)|m\rangle_{ph} + \tilde{\rho}_s(t)_{ph}\langle 0|\tilde{H}_I^L(\tau)|m\rangle_{ph}\ {}_{ph}\langle m|\tilde{H}_I^L(t)|0\rangle_{ph}\Big]. \tag{11}$$

We choose the basis $\{|10\rangle, |01\rangle\}$ for our analysis and obtain the following useful expressions:

$$e^{-iH_s^L t}|10\rangle = [p(t)^*|10\rangle - i\kappa q(t)|01\rangle]e^{i\frac{J_\parallel}{4}t} \tag{12}$$

and

$$e^{-iH_s^L t}|01\rangle = [p(t)|01\rangle - i\kappa q(t)|10\rangle]e^{i\frac{J_\parallel}{4}t}, \tag{13}$$

where $p(t) = \cos(t\sqrt{\frac{\Delta\varepsilon^2}{4}+\kappa^2}) + i\frac{\Delta\varepsilon}{2}\frac{\sin(t\sqrt{\frac{\Delta\varepsilon^2}{4}+\kappa^2})}{\sqrt{\frac{\Delta\varepsilon^2}{4}+\kappa^2}}$, $q(t) = \frac{\sin(t\sqrt{\frac{\Delta\varepsilon^2}{4}+\kappa^2})}{\sqrt{\frac{\Delta\varepsilon^2}{4}+\kappa^2}}$, and $\kappa = -\frac{J_\perp e^{-g^2}}{2}$. In addition, we also evaluate the matrix element

$${}_{ph}\langle 0|H_I^L|n\rangle_{ph} = \kappa(-1)^{n_1}\sqrt{C_n}(b_1^\dagger b_2 + (-1)^{n_1+n_2}b_2^\dagger b_1), \tag{14}$$

where $C_n = \frac{g^{2(n_1+n_2)}}{n_1!n_2!}$. Taking the matrix elements, with respect to $|10\rangle$ and $|01\rangle$, on both sides of Eq. (11) and by using Eqs. (12)–(14), we calculate the matrix elements of the four terms on the right-hand side of Eq. (11) (with details being shown in the Supplemental Material [22]). For the case when $|\Delta\varepsilon| \gg |\kappa|$, $|10\rangle$ and $|01\rangle$ are the approximate eigenstates of H_s^L. In this regime of parameter values, we ignore the ratio $\frac{|\kappa|}{|\Delta\varepsilon|}$ compared to 1 and finally obtain the simple form of the master equation for $\langle 10|\tilde{\rho}_s(t)|01\rangle$:

$$\frac{d\langle 10|\tilde{\rho}_s(t)|01\rangle}{dt} = -i\kappa^2 {\sum_n}' C_n \Bigg[\langle 10|\tilde{\rho}_s(t)|01\rangle \left(\frac{e^{-i(\omega_n-\Delta\varepsilon-i\eta)t}}{\omega_n-\Delta\varepsilon} - \frac{e^{i(\omega_n+\Delta\varepsilon+i\eta)t}}{\omega_n+\Delta\varepsilon} - \frac{2\Delta\varepsilon}{\omega_n^2-\Delta\varepsilon^2}\right)$$
$$+\langle 01|\tilde{\rho}_s(t)|10\rangle(-1)^{n_1+n_2}e^{i(2\Delta\varepsilon+i\eta)t}\left(\frac{e^{i(\omega_n-\Delta\varepsilon)t}}{\omega_n-\Delta\varepsilon} - \frac{e^{-i(\omega_n+\Delta\varepsilon)t}}{\omega_n+\Delta\varepsilon} - \frac{2\Delta\varepsilon}{\omega_n^2-\Delta\varepsilon^2}\right)\Bigg], \tag{15}$$

and its complex-conjugate equation for $\langle 01|\tilde{\rho}_s(t)|10\rangle$. In the above equation, ${\sum_n}' \equiv {\sum_{n_1,n_2}}'$ excludes the case where n_1 and n_2 are simultaneously zero. Similarly, for the diagonal element $\langle 10|\tilde{\rho}_s(t)|10\rangle$, the differential equation can be written as

$$\frac{d\langle 10|\tilde{\rho}_s(t)|10\rangle}{dt} = -2\kappa^2 {\sum_n}' C_n e^{-\eta t}\left[\langle 10|\tilde{\rho}_s(t)|10\rangle\left(\frac{\sin(\omega_n+\Delta\varepsilon)t}{\omega_n+\Delta\varepsilon} + \frac{\sin(\omega_n-\Delta\varepsilon)t}{\omega_n-\Delta\varepsilon}\right) - \frac{\sin(\omega_n+\Delta\varepsilon)t}{\omega_n+\Delta\varepsilon}\right]. \tag{16}$$

In Eqs. (15) and (16), we multiplied the oscillatory terms with a decay term $e^{-\eta t}$ (where $\eta \to +0$) to obtain the behavior of the matrix elements of $\tilde{\rho}_s(t)$ at long times, i.e., at times much larger than the largest time scale in the process $\hbar/J_\perp e^{-g^2}$.

To understand decoherence and the decay of the excited state ($|10\rangle$), we define two quantities: the coherence factor $\mathrm{C}(t) = \frac{|\langle 10|\rho_s(t)|01\rangle|}{|\langle 10|\rho_s(0)|01\rangle|}$ and the population of the excited state $\mathrm{P}(t) = \langle 10|\rho_s(t)|10\rangle$. We numerically solve the coupled differential equations given by Eq. (15) and its complex-conjugate equation and plot the dynamical behavior of $\mathrm{C}(t)$ in Figs. 2, 5(a), and 6. We also depict the time dependence of $\mathrm{P}(t)$ in Figs. 4, 5(b), and 7. We analyze below Figs. 2–7 and show that the period of oscillation and the amplitude of oscillation of both $\mathrm{C}(t)$ and $\mathrm{P}(t)$ increase as the site energy difference $\Delta\varepsilon$ approaches a harmonic ω_n; also, the closer the $\Delta\varepsilon$ is to ω_n, the smaller are the equilibrium values of $\mathrm{C}(t)$ and $\mathrm{P}(t)$. Furthermore, the closer ω_n is to $2g^2\omega$ (i.e., twice the polaronic energy), the more prominent are the period and amplitude of oscillations. Interestingly too, we find that the stronger the coupling g, the weaker is the decoherence and the decay of the excited-state population.

In Figs. 2 and 4, we study three cases of proximity of $\Delta\varepsilon$ to ω_n: $\frac{\Delta\varepsilon}{\omega} = 2.5, 7.5$, and 14.5; $\frac{\Delta\varepsilon}{\omega} = 2.9, 7.9$, and 14.9; and $\frac{\Delta\varepsilon}{\omega} = 3.0, 8.0$, and 15.0. One can see from Eq. (15) that, for values of $\Delta\varepsilon$ close to ω_n (i.e., for $\frac{\Delta\varepsilon}{\omega} = 2.9, 7.9$, and 14.9), the dominant terms have arguments of the periodic functions being given by $(\omega_n - \Delta\varepsilon)t = 0.1\omega t$; consequently, there is a large period of oscillation ($=20\pi/\omega$) in Fig. 2(b). Also, the amplitude of oscillation is dominated by the term $\sin[(\omega_n - \Delta\varepsilon)t]/(\omega_n - \Delta\varepsilon)$ and hence the amplitude increases with decreasing values of $(\omega_n - \Delta\varepsilon)$. Furthermore, the coherence factor also depends on the number of degenerate phonon states with eigenenergy ω_n; the contribution of this degeneracy [as seen from Eq. (15)] is determined by the term

$$\mathbb{C}^{\mathbb{N}} = \frac{\kappa^2}{\omega^2} \sum_{n_1,n_2;(n_1+n_2)=\mathbb{N}} C_n = \frac{\kappa^2}{\omega^2}\frac{(2g^2)^{\mathbb{N}}}{\mathbb{N}!}, \tag{17}$$

where $\sum_{n_1,n_2;(n_1+n_2)=\mathbb{N}}$ adds up all C_n with $(n_1+n_2) = \mathbb{N}$. The closeness of $\Delta\varepsilon$ to ω_n and the value of $\mathbb{C}^{\mathbb{N}}$ together determine the strength of decoherence. The value of $\mathbb{C}^{\mathbb{N}}$ increases with increasing $\mathbb{N} = n_1 + n_2$ up to some limit as depicted in Fig. 1.

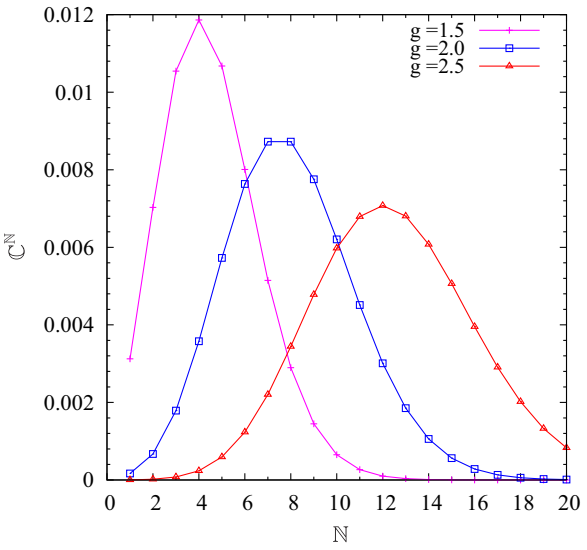

FIG. 1. (Color online) $\mathbb{C}^{\mathbb{N}}$ as a function of $\mathbb{N}$ for different values of coupling g and for $\frac{J_\perp}{\omega} = 0.5$.

One can also see that the maximum of $\mathbb{C}^{\mathbb{N}}$ occurs at phonon eigenenergy ω_n close to $2g^2\omega$. In other words, for a particular g, when $\Delta\varepsilon$ is close to twice the polaronic energy $g^2\omega$, decoherence is maximum with ω_n closest to $2g^2\omega$ making the dominant contribution. For a further understanding of the maximum value of $\mathbb{C}^{\mathbb{N}}$, see the explanation of Fig. 14 in Appendix B.

The above observations that the period of oscillation being inversely proportional to $\Delta\varepsilon - \omega_n$ and that the values of $1/(\Delta\varepsilon - \omega_n)$ and $\mathbb{C}^{\mathbb{N}}$ together determine the strength of decoherence are also exemplified for the cases when $\Delta\varepsilon = \omega_n$ [through Fig. 2(c) when $\frac{\Delta\varepsilon}{\omega} = 3.0, 8.0$, and 15.0] and when $|\Delta\varepsilon - \omega_n| = \omega/2$ [through Fig. 2(a) when $\frac{\Delta\varepsilon}{\omega} =$ 2.5,7.5, and 14.5]. In Fig. 2(c) [2(a)], the period of oscillation is infinity ($4\pi/\omega$) and the decoherence is stronger (weaker) than in Fig. 2(b). It should be clear that recoherence occurs in Fig. 2 because we are dealing with single-mode phonons; the closer that $\Delta\varepsilon$ approaches ω_n, the later does the recoherence occur (i.e., recoherence time is inversely proportional to $\Delta\varepsilon - \omega_n$).

Similar to the above analysis of Eq. (15), one can analyze Eq. (16) to gain an understanding of P(t). For comparatively large initial values $\langle 10|\rho_s(0)|10\rangle$, the time dependence of $\langle 10|\rho_s(t)|10\rangle$ is mainly determined by the homogeneous part in Eq. (16). The role of the inhomogeneous term can be understood from Fig. 3 by taking P(0) = 0 in the solution of Eq. (16). One can see a very small variation of the excited-state population and the peak values of oscillations in Fig. 3 are less than the order of $\frac{|\kappa|}{|\Delta\varepsilon|}$ [i.e., $\sim O(10^{-2})$]; we have neglected $\frac{|\kappa|}{|\Delta\varepsilon|}$ compared to 1 in our calculations. So [when P(0) = 0], we can say that the system stays in the ground state for all practical purposes. Next, in Eq. (16), we see that the homogeneous part is dominated by the oscillatory terms with period of oscillation being inversely proportional to $\Delta\varepsilon - \omega_n$; here too the values of $1/(\Delta\varepsilon - \omega_n)$ and $\mathbb{C}^{\mathbb{N}}$ together determine the strength of decay of P(t) as can be seen from Figs. 4(a)–4(c).

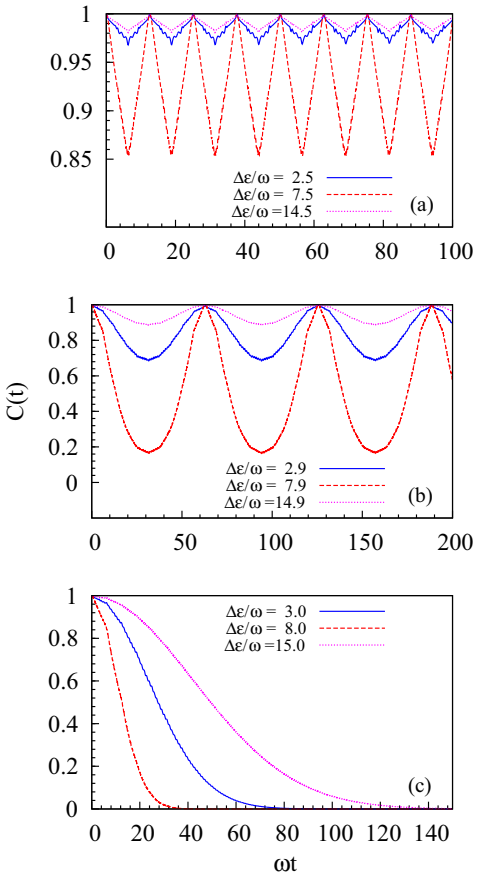

FIG. 2. (Color online) Time dependence of C(t) for $\frac{J_\perp}{\omega} = 0.5$, $g = 2.0$, and when (a) $\frac{\Delta\varepsilon}{\omega} = 2.5$, 7.5, and 14.5; (b) $\frac{\Delta\varepsilon}{\omega} = 2.9$, 7.9, and 14.9; and (c) $\frac{\Delta\varepsilon}{\omega} = 3.0, 8.0$ and 15.0.

To understand the dependence of C(t) and P(t) on the strength of coupling, we study the variation of $\mathbb{C}^{\mathbb{N}}$ on g in Fig. 1. The peak value of $\mathbb{C}^{\mathbb{N}}$ decreases with increasing g, i.e., the maximum decoherence/decay (which occurs when $\Delta\varepsilon = 2g^2\omega$) decreases as the coupling becomes stronger. In Figs. 5(a) and 5(b), respectively, C(t) and P(t) are plotted for different values of g with $\frac{\Delta\varepsilon}{\omega}$ taking integer values closest to $2g^2$.

Now, using Eqs. (15) and (16), we will determine the values of C(t) and P(t) at long times, i.e., at times much larger than the largest time scale in the process $\hbar/J_\perp e^{-g^2}$. We plot C(t) and

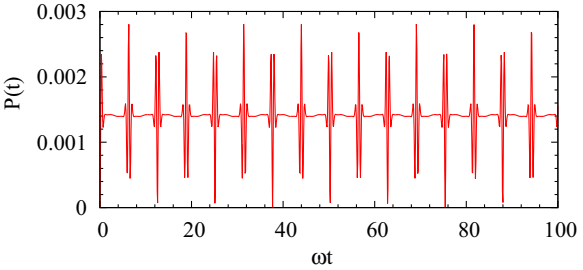

FIG. 3. (Color online) Time dependence of P(t) for $\frac{\Delta\varepsilon}{\omega} = 2.5$ when $\frac{J_\perp}{\omega} = 0.5$, P(0) = 0, and $g = 2.0$.

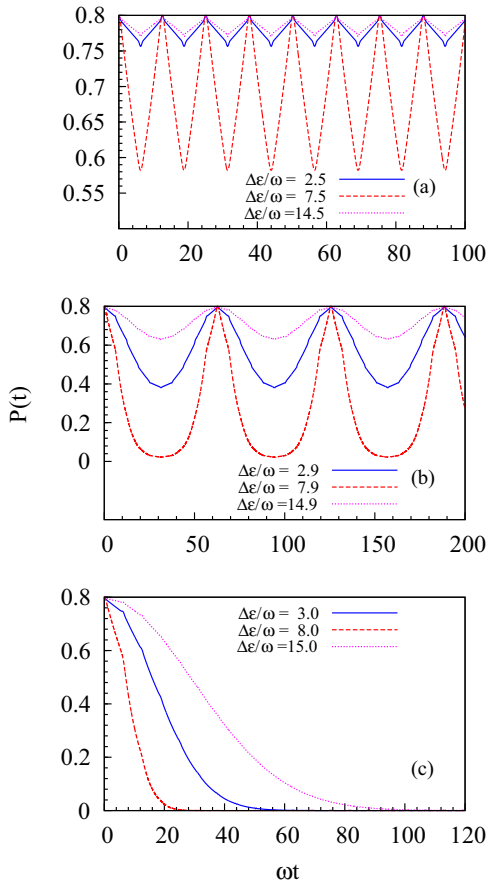

FIG. 4. (Color online) Time dependence of P(t) for $\frac{J_\perp}{\omega} = 0.5$, P(0) = 0.8, $g = 2.0$, and when (a) $\frac{\Delta\varepsilon}{\omega} = 2.5$, 7.5, and 14.5; (b) $\frac{\Delta\varepsilon}{\omega} = 2.9$, 7.9, and 14.9; and (c) $\frac{\Delta\varepsilon}{\omega} = 3.0$, 8.0, and 15.0.

P(t) in Figs. 6 and 7, respectively, for values of $\eta/\omega = 0.01$ and 0.02. For both the values of η, C(t) [as well as P(t)] attains the same equilibrium value. Here, we should mention that (for the chosen values of $\eta/\omega = 0.01$ and 0.02) although the decay

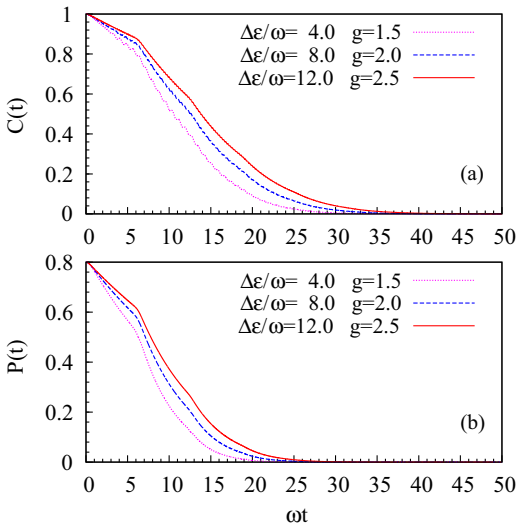

FIG. 5. (Color online) Time dependence of (a) C(t) and (b) P(t) [with P(0) = 0.8] for different values of coupling g and $\frac{J_\perp}{\omega} = 0.5$ when $\Delta\varepsilon/\omega$ takes integer values closest to $2g^2$.

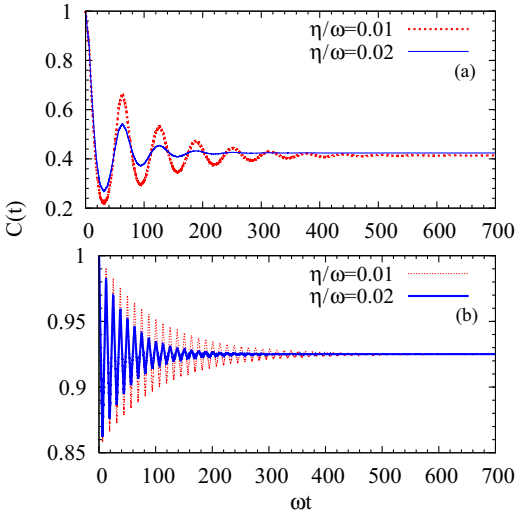

FIG. 6. (Color online) Time dependence of C(t) for $\frac{J_\perp}{\omega} = 0.5$, $g = 2.0$, and when (a) $\frac{\Delta\varepsilon}{\omega} = 7.9$ and (b) $\frac{\Delta\varepsilon}{\omega} = 7.5$.

term $e^{-\eta t}$ does diminish over the period of oscillation of C(t) and P(t), we got the same equilibrium values for much smaller values of η as well.

Lastly, we would like to compare the case of nonzero $\Delta\varepsilon$ with the case of $\Delta\varepsilon = 0$ using the plots in Figs. 8 and 9. To analyze decoherence using C(t) and decay of P(t), for each case, we use the corresponding eigenstate basis, i.e., $\{|10\rangle, |01\rangle\}$ for $\Delta\varepsilon \neq 0$ and $\{\frac{|10\rangle - |01\rangle}{\sqrt{2}}, \frac{|10\rangle + |01\rangle}{\sqrt{2}}\}$ for $\Delta\varepsilon = 0$; we note that $\frac{|10\rangle - |01\rangle}{\sqrt{2}}$ is the excited state for the case of $\Delta\varepsilon = 0$. We see that the periodicity of the cases with nonzero site energy [depicted in Figs. 2, 4, 8(a), and 9(a)] is determined by the closeness of $\Delta\varepsilon$ to ω_n whereas the periodicity of the case with $\Delta\varepsilon = 0$ is determined by ω. For the case of $\Delta\varepsilon = 0$, in the strong coupling regime, since the system excitation energy $J_\perp e^{-g^2}$ is much smaller than ω, there is no possibility of energy

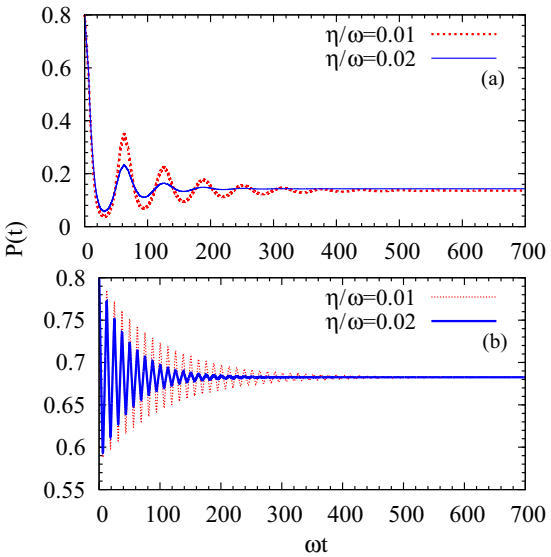

FIG. 7. (Color online) Time dependence of P(t) for $\frac{J_\perp}{\omega} = 0.5$, P(0) = 0.8, $g = 2.0$, and when (a) $\frac{\Delta\varepsilon}{\omega} = 7.9$ and (b) $\frac{\Delta\varepsilon}{\omega} = 7.5$.

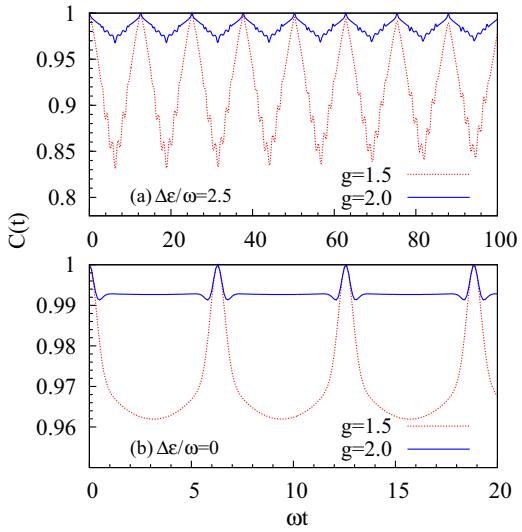

FIG. 8. (Color online) Time dependence of C(t) for $\frac{J_\perp}{\omega} = 0.5$, $g = 1.5$, and 2.0, and when (a) $\frac{\Delta\varepsilon}{\omega} = 2.5$ and (b) $\frac{\Delta\varepsilon}{\omega} = 0$.

exchange between the system and phonons. This results in smaller equilibrium values of C(t) and P(t) for the case with finite $\Delta\varepsilon$ compared to the case with $\Delta\varepsilon = 0$ as shown in Table I. Also, the oscillations of C(t) and P(t) are smaller for the case $\Delta\varepsilon = 0$ compared to the case of finite $\Delta\varepsilon$ as can be seen by comparing Figs. 8(b) and 9(b) with Figs. 8(a) and 9(a); here we chose $\Delta\varepsilon/\omega = 2.5$ so that $\Delta\varepsilon$ is far away from the nearest eigenenergies $\omega_n = 2\omega$ and 3ω. Furthermore, in Fig. 8(b) [Fig. 9(b)] the ωt regions between two consecutive integer multiples of 2π (π) become flatter as the coupling g increases; as g increases, more number of excited states for phonons (with energy ω_n) contribute and produce destructive interference of phases resulting in the flat region (see Ref. [5] for details) [23]. On the other hand, in Figs. 8(a) and 9(a), only those states with ω_n close to $\Delta\varepsilon$ have a dominant contribution.

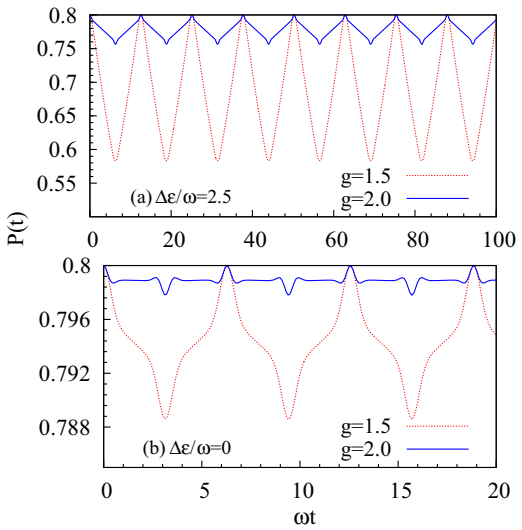

FIG. 9. (Color online) Time dependence of P(t) for $\frac{J_\perp}{\omega} = 0.5$, P(0) = 0.8, $g = 1.5$ and 2.0, and when (a) $\frac{\Delta\varepsilon}{\omega} = 2.5$ and (b) $\frac{\Delta\varepsilon}{\omega} = 0$.

TABLE I. Equilibrium values of C(t) and P(t) [with P(0) = 0.8] for $J_\perp/\omega = 0.5$ and various values of g when $\Delta\varepsilon/\omega = 0$,2.5 and 2.9.

$\Delta\varepsilon/\omega$ / g	0		2.5		2.9	
	C(∞)	P(∞)	C(∞)	P(∞)	C(∞)	P(∞)
1.5	0.970	0.794	0.916	0.683	0.343	0.096
2.0	0.993	0.799	0.984	0.778	0.830	0.555

Thus, to minimize decoherence and dissipation, it is desirable to set the site-energy difference to be much smaller than the phonon frequency.

In principle, the model (dealt with in this section) can be extended to a many-site, many-body HCB system. However, with increasing system size, the growing Hilbert space of the system makes the analytical treatment more cumbersome and difficult; we still expect a low degree of decoherence unless the site-energy difference between any two sites does match with the phonon eigenenergy. In the future, we would like to carry out the above analysis for a smaller system of three (or four) sites.

III. INFINITE-RANGE HCB MODEL WITH HCBs COUPLED TO LOCAL OPTICAL PHONONS

In this section, we analyze an extreme long-range many-body HCB model with equal site energies. Having equal site energies not only makes the model analytically tractable, but can also be helpful to attain long-range interactions; in a cavity QED, multiqubit architecture has been proposed and it was shown that one can get sizable qubit-qubit interaction over large distances when both the qubits have the same energy [8,11]. Moreover, we have shown that decoherence and dissipation are quite small when site-energy difference is negligible compared to the phonon frequency (see previous section and Ref. [5]). We begin by introducing the infinite-range HCB model whose decoherence will be studied when the system is coupled to local phonons. The Hamiltonian for that is defined as

$$H_{\rm HCB} = \sum_{i,j>i}\left[\frac{-J_\perp}{2}(b_i^\dagger b_j + {\rm H.c.}) + J_\parallel\left(n_i - \frac{1}{2}\right)\left(n_j - \frac{1}{2}\right)\right]. \tag{18}$$

It is understood that $J_\perp = J_\perp^\star/(N-1)$ and $J_\parallel = J_\parallel^\star/(N-1)$ (where $J_\perp^\star$ and $J_\parallel^\star$ are finite quantities) so that the energy per site remains finite as $N \to \infty$. The total Hamiltonian is defined by

$$H_T = \sum_{i,j>i}\left[\frac{-J_\perp}{2}(b_i^\dagger b_j + {\rm H.c.}) + J_\parallel\left(n_i - \frac{1}{2}\right)\left(n_j - \frac{1}{2}\right)\right] + \omega\sum_j a_j^\dagger a_j + g\omega\sum_j\left(n_j - \frac{1}{2}\right)(a_j + a_j^\dagger). \tag{19}$$

Subsequently, we perform the LF transformation

$$H_T^L \equiv e^S H_T e^{-S} = H_0^L + H_I^L, \tag{20}$$

where again $S = -g\sum_i(n_i - \frac{1}{2})(a_i - a_i^\dagger)$. Next, the unperturbed Hamiltonian H_0^L is expressed as

$$H_0^L = H_s^L + H_{\rm env}^L, \tag{21}$$

where we identify H_s^L as the system Hamiltonian

$$H_s^L = \sum_{i,j>i}\left[\frac{-J_\perp}{2}e^{-g^2}(b_i^\dagger b_j + \text{H.c.}) + J_\parallel\left(n_i - \frac{1}{2}\right)\left(n_j - \frac{1}{2}\right)\right], \tag{22}$$

and $H_{\rm env}^L$ as the Hamiltonian of the environment

$$H_{\rm env}^L = \omega\sum_j a_j^\dagger a_j. \tag{23}$$

On the other hand, the interaction H_I^L (which we will treat as perturbation) is given by

$$H_I^L = -\frac{1}{2}\sum_{i,j>i}[J_{ij}^\pm b_i^\dagger b_j + \text{H.c.}], \tag{24}$$

where $J_{ij}^\pm/J_\perp = e^{\pm g[(a_j - a_j^\dagger) - (a_i - a_i^\dagger)]} - e^{-g^2}$ is the local phonon fluctuation (at sites i and j) about the mean phonon field e^{-g^2}. In the transformed frame, the system Hamiltonian H_s^L depicts that all the HCBs are coupled to the same phononic mean field. Thus, the unperturbed Hamiltonian H_0^L comprises of the system Hamiltonian H_s^L representing HCBs with the same reduced hopping term $\frac{1}{2}J_\perp e^{-g^2}$ and the environment Hamiltonian $H_{\rm env}^L$ involving displaced bath oscillators corresponding to local distortions. Here, it should be pointed out that the mean-field term H_s^L involves controlled degrees of freedom. Thus, no irreversibility is involved under evolution due to H_0^L. On the other hand, perturbation H_I^L pertains to the interaction of HCBs with local deviations from the phononic mean field; the interaction term H_I^L represents numerous or uncontrolled environmental degrees of freedom and thus has the potential for producing decoherence. Furthermore, it is of interest to note that the interaction term is weak in the transformed frame unlike the interaction in the original frame; thus, one can perform perturbation theory with the interaction term. We represent the eigenstates of the unperturbed Hamiltonian H_0^L as $|n,m\rangle \equiv |n\rangle_s \otimes |m\rangle_{ph}$ with the corresponding eigenenergies $E_{n,m}^{(0)} = E_n^s + E_m^{ph}$; $|n\rangle_s$ is the eigenstate of the system with eigenenergy E_n^s, while $|m\rangle_{ph}$ is the eigenstate for the environment with eigenenergy E_m^{ph}. Henceforth, for brevity, we will use $\omega_m \equiv E_m^{ph}$. Next, we observe that $\langle n,0|H_I^L|n,0\rangle = 0$ because ${}_{ph}\langle 0|J_{ij}^\pm|0\rangle_{ph} = 0$. Then, corresponding to the unperturbed eigenenergy $E_{n,0}^{(0)}$, the next relevant second-order perturbation term $E_{n,0}^{(2)}$ is given as follows (see Appendix A of Ref. [24]):

$$E_{n,0}^{(2)} = \sum_{l,m}\frac{\langle n,0|H_I^L|l,m\rangle\langle l,m|H_I^L|n,0\rangle}{E_{n,0}^{(0)} - E_{l,m}^{(0)}} \approx \sum_m \frac{\langle n,0|H_I^L|m\rangle_{ph}\,{}_{ph}\langle m|H_I^L|n,0\rangle}{\omega_0 - \omega_m}, \tag{25}$$

where use has been made of the fact that $|E_n^s - E_l^s| \leqslant J_\perp^\star e^{-g^2}$ (as shown in the next section) and that $J_\perp^\star e^{-g^2} \ll \omega$ as follows from the conditions of strong coupling (i.e., $g^2 \gg 1$) [25] and nonadiabaticity (i.e., $J_\perp^\star/\omega \leqslant 1$) [26] assumed in this paper; we also noted that $\omega_m - \omega_0 = \omega_m$ is a positive integral multiple of ω. Using Schrieffer-Wolff (SW) transformation (as elaborated in Appendix A of Refs. [24,27]), we get the following second-order term $H^{(2)}$ (see Ref. [28]):

$$H^{(2)} = -\sum_m \frac{{}_{ph}\langle 0|H_I^L|m\rangle_{ph}\,{}_{ph}\langle m|H_I^L|0\rangle_{ph}}{\omega_m} = \sum_{i,j>i}\left[\left(\frac{1}{2}J_\perp^{(2)}b_i^\dagger b_j + \text{H.c.}\right) - \frac{1}{2}J_\parallel^{(2)}\{n_i(1-n_j) + n_j(1-n_i)\}\right], \tag{26}$$

where

$$J_\perp^{(2)} \equiv -(N-2)f_1(g)\frac{J_\perp^2 e^{-2g^2}}{2\omega} \sim -(N-2)\frac{J_\perp^2 e^{-g^2}}{2g^2\omega}, \tag{27}$$

$$J_\parallel^{(2)} \equiv [2f_1(g) + f_2(g)]\frac{J_\perp^2 e^{-2g^2}}{2\omega} \sim \frac{J_\perp^2}{4g^2\omega}, \tag{28}$$

with $f_1(g) \equiv \sum_{l=1}^\infty g^{2l}/(l!l)$ and $f_2(g) \equiv \sum_{j=1}^\infty\sum_{l=1}^\infty g^{2(j+l)}/[j!l!(j+l)]$. The effective Hamiltonian $H_s^L + H^{(2)}$ is a low-energy Hamiltonian obtained by the canonical SW transformation [29,30] decoupling the low- and the high-energy subspaces; this decoupling is a consequence of $J_\perp^\star e^{-g^2} \ll \omega$. We now make the important observation that the effective Hamiltonian $H_s^L + H^{(2)}$ has the same set of eigenstates as those of H_s^L and $H_{\rm HCB}$ because $\sum_{i,j>i}(n_i - \frac{1}{2})(n_j - \frac{1}{2})$ commutes with both H_s^L and $H_{\rm HCB}$. Actually, we have shown that even in higher-order perturbation theory (higher than second order) the eigenstates of the effective Hamiltonian do not change [31]. The small parameter of our perturbation theory, for a small-N system, is $\frac{J_\perp}{2g\omega}$ (see Ref. [32] for details); whereas for a large N, the small parameter is $\frac{J_\perp^\star}{g^2\omega}$ (see Ref. [33] for an explanation). It is the long range of the model that enables the eigenstates of the system to remain unchanged. While the fact that the eigenstates of the effective Hamiltonian remain the same as those of $H_{\rm HCB}$ may be suggestive of the robustness of the states of this long-range model, to establish that the states of the system are actually decoherence free, it is necessary to show that the off-diagonal matrix elements of the system's reduced density matrix do not diminish. Next, we study decoherence in a dynamical context and gain more insight into how the states of our $H_{\rm HCB}$ can be decoherence free.

A. Dynamical evolution of the system

In this section, we will study decoherence in the system from the dynamical perspective. Although the eigenstates of the effective Hamiltonian and $H_{\rm HCB}$ are the same, the system-environment interaction may lead to certain correlations such that the resulting state of the system may no longer be represented in terms of unitary Hamiltonian dynamics.

We begin by observing that, to understand decoherence in the original frame of reference where the HCB-phonon coupling is strong, it is convenient to use the LF transformed frame of reference. The relevant Hamiltonian (for our decoherence analysis) is the following LF transformed Hamiltonian:

$$H_T^{\mathrm{L}} = H_0^L + H_I^L, \tag{29}$$

where H_0^L is the system-environment Hamiltonian given by Eq. (21) and H_I^L represents the interaction Hamiltonian given by Eq. (24). As before, here too the initial state of the total system is taken to be a factorized (or simply separable) state given by $\rho_T(0) = \rho_s(0) \otimes R_0$ where $R_0 = \sum_n |n\rangle_{ph\ ph}\langle n|e^{-\beta\omega_n}/Z$; also, here too $\rho_s(0)$ need not represent only the ground state. Such a factorized state can be prepared, as in the case of oxide-based DQD, by using small values of $J_\perp/\omega$ (i.e., $\lesssim 10^{-3}$). Once a separable state is prepared, one can rapidly alter the interaction $J_\perp$ to the desired value before any HCB hops.

Next, we will study the Markovian dynamics of the system. The Markov approximation is valid when the correlation time scale τ_c for the environmental fluctuations is negligibly small compared to the relaxation time scale τ_s for the system, i.e., $\tau_c \ll \tau_s$. Furthermore, it has been shown that the Markov approximation becomes more valid for stronger coupling g and enhanced nonadiabaticity, i.e., for smaller values of the small parameter (see Ref. [5] and Appendix B); this result follows because τ_c/τ_s can be approximated by the square of the small parameter. The Markov approximation (with $\tau_c \ll \tau_s$) allows us to use the second-order time-convolutionless Markovian master equation (see Ref. [21] for further details)

$$\frac{d\tilde{\rho}_s(t)}{dt} = -i\,\mathrm{Tr}_R\big[\tilde{H}_I^L(t), \rho_s(0)\otimes R_0\big] - \int_0^\infty d\tau\,\mathrm{Tr}_R\big[\tilde{H}_I^L(t), \big[\tilde{H}_I^L(t-\tau), \tilde{\rho}_s(t)\otimes R_0\big]\big]. \tag{30}$$

Now, by defining $\{|m\rangle_{ph}\}$ as the basis set for phonons and observing that, at 0 K temperature $\mathrm{Tr}_R[\tilde{H}_I^L(t), \rho_s(0)\otimes R_0] = 0$, we can write the master equation at zero temperature as

$$\begin{aligned}\frac{d\tilde{\rho}_s(t)}{dt} = -\sum_m \int_0^\infty d\tau \big[&{}_{ph}\langle 0|\tilde{H}_I^L(t)|m\rangle_{ph\ ph}\langle m|\tilde{H}_I^L(t-\tau)|0\rangle_{ph}\tilde{\rho}_s(t) - {}_{ph}\langle m|\tilde{H}_I^L(t)|0\rangle_{ph}\tilde{\rho}_s(t)_{ph}\langle 0|\tilde{H}_I^L(t-\tau)|m\rangle_{ph} \\ &- {}_{ph}\langle m|\tilde{H}_I^L(t-\tau)|0\rangle_{ph}\tilde{\rho}_s(t)_{ph}\langle 0|\tilde{H}_I^L(t)|m\rangle_{ph} + \tilde{\rho}_s(t)_{ph}\langle 0|\tilde{H}_I^L(t-\tau)|m\rangle_{ph\ ph}\langle m|\tilde{H}_I^L(t)|0\rangle_{ph}\big].\end{aligned} \tag{31}$$

In order to simplify the above master equation (31), we need to evaluate the various terms occurring on its right-hand side; considering the first term yields

$$\sum_m {}_{ph}\langle 0|\tilde{H}_I^L(t)|m\rangle_{ph\ ph}\langle m|\tilde{H}_I^L(t-\tau)|0\rangle_{ph}\tilde{\rho}_s(t) = \sum_m e^{iH_s^L t}\,{}_{ph}\langle 0|H_I^L|m\rangle_{ph}e^{-iH_s^L t}e^{iH_s^L(t-\tau)}\,{}_{ph}\langle m|H_I^L|0\rangle_{ph}e^{-iH_s^L(t-\tau)}\tilde{\rho}_s(t)e^{-i\omega_m\tau}. \tag{32}$$

We connect the HCBs in real space with those in momentum space as $b_j^\dagger = \frac{1}{\sqrt{N}}\sum_{k_1} e^{ik_1 r_j} b_{k_1}^\dagger$; henceforth, in momentum space, the creation and destruction operators of HCBs shall be denoted, respectively, as $b_{k_n}^\dagger$ and b_{k_n} with $n = 1,2,3,\ldots$. Then, it is important to note that the hopping term in the system Hamiltonian can be written as (see Refs. [28,34])

$$\frac{1}{2}J_\perp e^{-g^2}\sum_{i,j>i}(b_i^\dagger b_j + \mathrm{H.c.}) = \frac{1}{2}J_\perp e^{-g^2}\left[\sum_{i,j} b_i^\dagger b_j - \sum_i b_i^\dagger b_i\right] = \frac{1}{2}J_\perp e^{-g^2}[N\hat{n}_0 - \hat{N}_p] = \sum_{k_1}\epsilon_{k_1} b_{k_1}^\dagger b_{k_1}, \tag{33}$$

where $J_\perp = J_\perp^\star/(N-1)$, $\hat{N}_p \equiv \sum_{k_1} b_{k_1}^\dagger b_{k_1}$, and $\hat{n}_0 \equiv b_0^\dagger b_0$ (i.e., the particle number in momentum $k_1 = 0$ state). Thus, the single-particle energy (obtained from hopping) is given by

$$\epsilon_{k_1} = \frac{1}{2}J_\perp^\star\frac{N}{N-1}e^{-g^2}\delta_{k_1,0} - \frac{1}{2}J_\perp e^{-g^2}. \tag{34}$$

We take the total number of HCBs to be conserved; then, only the hopping term in H_s^L will contribute to the change in the system energy [see Eq. (22)]. Thus, in Eq. (25), the largest value of the change in system energy in the denominator is given by the following maximum change in the single-particle energy:

$$\left|E_n^s - E_l^s\right| = \frac{1}{2}J_\perp^\star\frac{N}{N-1}e^{-g^2}, \tag{35}$$

which is N times the hopping term $(1/2)J_\perp e^{-g^2}$ in H_s^L. Let $\{|q\rangle_s\}$ denote the complete set of energy eigenstates (with eigenenergies E_q^s) of the system Hamiltonian H_s^L; then we can write

$$e_{ph}^{iH_s^L t}\langle n|H_I^L|m\rangle_{ph}e^{-iH_s^L t} = \sum_{q,q'}|q\rangle_{ss}\langle q|_{ph}\langle n|H_I^L|m\rangle_{ph}|q'\rangle_{ss}\langle q'|e^{i(E_q^s - E_{q'}^s)t}, \tag{36}$$

where $|E^s_q - E^s_{q'}| \leqslant \frac{1}{2}J^\star_\perp(\frac{N}{N-1})e^{-g^2}$ [based on Eq. (35)]. Substituting Eq. (36) in Eq. (32), we get

$$\sum_m {}_{ph}\langle 0|\tilde{H}^L_I(t)|m\rangle_{ph}\,{}_{ph}\langle m|\tilde{H}^L_I(t-\tau)|0\rangle_{ph}\tilde{\rho}_s(t)$$
$$= \sum_m \sum_{q,q',q''} \left[|q\rangle_{ss}\langle q|_{ph}\langle 0|H^L_I|m\rangle_{ph}|q'\rangle_{ss}\langle q'|_{ph}\langle m|H^L_I|0\rangle_{ph}|q''\rangle_{ss}\langle q''|e^{i[(E^s_q-E^s_{q'})t+(E^s_{q'}-E^s_{q''})(t-\tau)]}\right]\tilde{\rho}_s(t)e^{-i\omega_m\tau}. \quad (37)$$

Since $J^\star_\perp e^{-g^2} \ll \omega$ and since the maximum value of $|E^s_{q'} - E^s_{q''}| \leqslant J^\star_\perp e^{-g^2}$ as well as the maximum value of $|E^s_q - E^s_{q'}| \leqslant J^\star_\perp e^{-g^2}$, the following are valid approximations:

$$e^{i(t-\tau)[\omega_m+(E^s_{q'}-E^s_{q''})]} \approx e^{i(t-\tau)\omega_m} \quad (38)$$

and

$$e^{it[-\omega_m+(E^s_q-E^s_{q'})]} \approx e^{-it\omega_m}, \quad (39)$$

where ω_m is a positive integral multiple of ω. The above approximations imply that we do not get terms producing decay. Then, on using the approximations given by Eqs. (38) and (39), Eq. (37) simplifies to be

$$\sum_m {}_{ph}\langle 0|\tilde{H}^L_I(t)|m\rangle_{ph}\,{}_{ph}\langle m|\tilde{H}^L_I(t-\tau)|0\rangle_{ph}\tilde{\rho}_s(t) = \sum_m {}_{ph}\langle 0|H^L_I|m\rangle_{ph}\,{}_{ph}\langle m|H^L_I|0\rangle_{ph}\tilde{\rho}_s(t)e^{-i\omega_m\tau}. \quad (40)$$

Carrying out the same analysis on the remaining (i.e., second, third, and fourth) terms in the master equation, we write Eq. (31) as

$$\frac{d\tilde{\rho}_s(t)}{dt} = -\sum_n \left[\int_0^\infty d\tau\, e^{-i(\omega_n-i\eta)\tau}|{}_{ph}\langle 0|H^L_I|n\rangle_{ph}|^2\tilde{\rho}_s(t) + \int_0^\infty d\tau\, e^{i(\omega_n+i\eta)\tau}\tilde{\rho}_s(t)|{}_{ph}\langle 0|H^L_I|n\rangle_{ph}|^2 - \int_{-\infty}^\infty d\tau\, e^{i\omega_n\tau}_{ph}\langle n|H^L_I|0\rangle_{ph}\tilde{\rho}_s(t)\,{}_{ph}\langle 0|H^L_I|n\rangle_{ph}\right], \quad (41)$$

where $\eta \to +0$. Now, we know that $\int_{-\infty}^\infty d\tau\, e^{i\omega_n\tau} \propto \delta(\omega_n)$. Therefore, on using this relation and the fact that ${}_{ph}\langle 0|H^L_I|0\rangle_{ph} = 0$, the third term in Eq. (41) vanishes; hence, we get

$$\frac{d\tilde{\rho}_s(t)}{dt} = i\sum_n \left[\frac{\left|{}_{ph}\langle 0|H^L_I|n\rangle_{ph}\right|^2}{\omega_n}\tilde{\rho}_s(t) - \tilde{\rho}_s(t)\frac{\left|{}_{ph}\langle 0|H^L_I|n\rangle_{ph}\right|^2}{\omega_n}\right]. \quad (42)$$

Here, it should be pointed out that the above simplified form for the master equation was possible due to the Markovian approximation made. Based on Eq. (26), we identify the term $-\sum_n[\frac{|{}_{ph}\langle 0|H^L_I|n\rangle_{ph}|^2}{\omega_n}]$ in the above equation to be the term $H^{(2)}$ obtained in second-order perturbation which together with H^L_s makes up the effective Hamiltonian (in second-order perturbation). On noting that $\tilde{\rho}_s(t) = e^{iH^L_s t}\rho_s(t)e^{-iH^L_s t}$ and that $H^{(2)}$ commutes with H^L_s (see Sec. III), it follows from Eq. (42) that

$$\frac{d\rho_s(t)}{dt} = -i\left[H^L_s + H^{(2)}, \rho_s(t)\right]. \quad (43)$$

The above Eq. (43) shows that the effective Hamiltonian $(H^L_s + H^{(2)})$ governs the unitary evolution of the reduced density matrix $\rho_s(t)$ with $\rho_s(t) = e^{-i(H^L_s+H^{(2)})t}\rho_s(0)e^{i(H^L_s+H^{(2)})t}$. Let $|n\rangle_s$ be the simultaneous eigenstate for $H^{(2)}$ and H^L_s with eigenvalues $E^{(2)}_n$ and E^s_n, respectively. Then, from the above Eq. (43) we get

$${}_s\langle n|\rho_s(t)|m\rangle_s = e^{-i(E_n-E_m)t}_s\langle n|\rho_s(0)|m\rangle_s, \quad (44)$$

where $E_n = E^s_n + E^{(2)}_n$. Thus, we see from the above equation that there is only a phase shift but no decoherence! Thus, up to second order in perturbation, the assumption $J^\star_\perp e^{-g^2} \ll \omega$, the long range of the model, the condition of equal site energies, and the Markov approximation together have ensured that the system, with a fixed $\sum_i n_i$, does not decohere; furthermore, the population ${}_s\langle n|\rho_s(t)|n\rangle_s$ does not change with time.

IV. DISCUSSION AND CONCLUSIONS

In this work, we considered two models of HCB that are characterized by strong HCB-phonon coupling and antiadiabaticity; the initial state of both the models contains no correlation between the system and the optical-phonon environment in the polaronic frame of reference (where the interaction term is weak). These two models are a generalization of the system studied in Ref. [5]. The case where site-energy differences can be comparable to the phonon eigenenergies needs to be analyzed using non-Markovian dynamics because the dominant interaction energy (resulting from second-order perturbation) need not be small compared to the phonon frequency. On the other hand, when the site energies are taken to be equal (as in cavity QED so as to produce sizable long-range interaction), one can restrict the largest interaction energy (by tuning the hopping term) to be significantly smaller than the phonon frequency, thereby ensuring Markovian dynamics.

First, for an amenable two-site system, we analyze the case where the site-energy difference is non-negligible compared

to the phonon energy. When the site-energy difference is (not) close to a phonon eigenenergy, the amount of decoherence and decay of excited state are (not) sizable. The extension of the model to a many-site case involves much more analytical complication and will be dealt with in the future. However, the analysis in Sec. II indicates a small decoherence as long as the site-energy difference between any two sites remains sufficiently away from the phonon eigenenergies.

Second, when the site energies are all equal, we have shown that an infinite-range HCB model subject to Markovian dynamics does not show decoherence or decay of excited-state population. It is the long-range nature of the Hamiltonian, the equal values for the site energies, and the negligible renormalized hopping (compared to the phonon frequency) that preserve the eigenstates of the system; in addition, when the small parameter is sufficiently small, Markov process can be assumed and then the dynamics is decoherence free.

We should mention that the approximate results obtained in Sec. II (by neglecting $\frac{|\kappa|}{|\Delta\varepsilon|}$ compared to 1) are very close to the results obtained without any approximation (i.e., using the full expressions given in the Supplemental Material [22]). Moreover, for the numerical results, we used fourth-order Runge-Kutta for solving differential equations and Gaussian quadrature for numerical integrations.

In the paper, we mainly dealt with the regime of strong coupling ($g^2 \gg 1$) and nonadiabaticity ($\frac{J_\perp}{\omega} \leqslant 1$); however, our results are valid even in the adiabatic regime $\frac{J_\perp}{\omega} > 1$ as long as the coupling g satisfies the condition $g^2 \gg (\frac{J_\perp}{\omega})^2$.

We will now make a few general remarks regarding the range of hopping in a multisite case. In contrast to our long-range model involving distance-independent hopping of HCBs, if we were to consider a chain with nearest-neighbor (NN) hopping [of the type $\sum_i \{\frac{-J_\perp}{2}(b_i^\dagger b_{i+1} + \text{H.c.}) + J_\parallel(n_i - \frac{1}{2})(n_{i+1} - \frac{1}{2})\}$ (with $J_\parallel = 0$)] and strongly couple the HCBs to local phonons [by introducing the additional terms $g\omega \sum_i (n_i - \frac{1}{2})(a_i^\dagger + a_i) + \omega \sum_i a_i^\dagger a_i$], we get decoherence for the case of half-filling. The NN-hopping system transits from a superfluid, with large values of the off-diagonal density matrix terms [i.e., $\langle b_i^\dagger \sum_{j\neq i} b_j\rangle$ = Bose-Einstein condensate occupation number $n_0 \propto \sqrt{N}$ (see Ref. [24])], to a charge-density-wave state with significantly diminished off-diagonal density matrix terms ($\langle b_i^\dagger \sum_{j\neq i} b_j\rangle$). The above analysis can be mapped (through a HCB-to-spin transformation and then a Wigner-Jordan transformation) on to the analysis in Ref. [16] dealing with the transition from a Luttinger liquid to a charge-density wave. Furthermore, the eigenstates of the effective Hamiltonian are not the same as the original NN-hopping model (for the $J_\parallel = 0$ case); the effective Hamiltonian contains additional next-nearest-neighbor hopping terms $b_{i+1}^\dagger b_{i-1}$ and additional NN repulsion terms $n_{i+1}n_i$ that are not present in the original Hamiltonian [see Eqs. (4) and (5) in Ref. [16]]. It is important to note that the infinite-range HCB model gives decoherence-free behavior, whereas the NN HCB model does not; thus, the range of interaction determines the decoherence of the system even when $J^\star e^{-g^2} \ll \omega$.

Although the analysis in this paper is valid for optical phonons, it can also accommodate acoustic phonons in small systems because the smallest wave vector, for a system with fixed boundaries, is inversely proportional to the system size; hence, for a small system $\Delta\varepsilon$ can be different from the eigenenergies of acoustic phonons. Lastly, the above analysis is valid in the regime $k_BT/\omega \ll 1$; the finite-temperature case $k_BT/\omega \gtrsim 1$ needs additional extensive considerations and will be dealt with elsewhere.

In the two-site case, the dynamics of population as well as the coherence are important for understanding physical systems such as a double quantum dot (DQD) acting as a qubit for quantum computation [5]. An oxide- (i.e., manganite-) based DQD [5], with negligible detuning, can serve as a charge qubit as it has very small decoherence compared to a semiconductor DQD; furthermore, it can also meet the demands of miniaturization as its size can also be much smaller than a semiconductor DQD [4]. Minimizing the decoherence in an interacting long-range, many-qubit system coupled to the environment is quite useful for developing quantum computer architecture; our analysis of an infinite-range, many-body HCB model with Markovian dynamics is a step to meet this end.

ACKNOWLEDGMENT

One of the authors (S.Y.) would like to thank G. Baskaran, P. B. Littlewood, R. Simon, S. Ghosh, and S. Reja for valuable discussions.

APPENDIX A: MULTIMODE CASE

Here, we deal with a more realistic case, i.e., we consider a continuous distribution of phonon frequencies and, for simplicity, allow a small window characterized by upper and lower limits. The generalized Hamiltonian for multimode phonons in the laboratory frame of reference is written as

$$H = \varepsilon_1\left(n_1 - \frac{1}{2}\right) + \varepsilon_2\left(n_2 - \frac{1}{2}\right) - \frac{J_\perp}{2}(b_1^\dagger b_2 + b_2^\dagger b_1) + J_\parallel\left(n_1 - \frac{1}{2}\right)\left(n_2 - \frac{1}{2}\right) + \sum_{i,k}\omega_k a_{i,k}^\dagger a_{i,k} + \frac{1}{\sqrt{N}}\sum_{i,k} g_k\omega_k\left(n_i - \frac{1}{2}\right)(a_{i,k} + a_{i,k}^\dagger), \tag{A1}$$

where $a_{i,k}$ destroys a phonon with momentum k at site i and N is the number of phonon modes. To perform perturbation theory with ease, we perform Lang-Firsov transformation $H^L = e^S H e^{-S} = H_s^L + H_{\text{env}}^L + H_I^L$ where $S = -\frac{1}{\sqrt{N}}\sum_{i,k} g_k(n_i - \frac{1}{2})(a_{i,k} - a_{i,k}^\dagger)$. Then, the components of H^L (i.e., the system part H_s^L, the environment part H_{env}^L, and the interaction part H_I^L) are expressed as

$$H_s^L = \varepsilon_1\left(n_1 - \frac{1}{2}\right) + \varepsilon_2\left(n_2 - \frac{1}{2}\right) + J_\parallel\left(n_1 - \frac{1}{2}\right)\left(n_2 - \frac{1}{2}\right) - \frac{J_\perp e^{-\frac{1}{N}\sum_k g_k^2}}{2}(b_1^\dagger b_2 + b_2^\dagger b_1), \tag{A2}$$

$$H_{\text{env}}^L = \sum_{i,k}\omega_k a_{i,k}^\dagger a_{i,k}, \tag{A3}$$

and

$$H_I^L = -\frac{1}{2}[J_\perp^+ b_1^\dagger b_2 + J_\perp^- b_2^\dagger b_1], \tag{A4}$$

where

$$J_\perp^\pm = J_\perp e^{\pm\frac{1}{\sqrt{N}}\sum_k g_k[(a_{2,k}-a_{2,k}^\dagger)-(a_{1,k}-a_{1,k}^\dagger)]} - J_\perp e^{-\frac{1}{N}\sum_k g_k^2}. \tag{A5}$$

Now, we use the non-Markovian master equation (11) to study the dynamics of the reduced density matrix. We calculate below the matrix element ${}_{ph}\langle\{0_1^k\},\{0_2^k\}|H_I^L|\{m_1^k\},\{m_2^k\}\rangle_{ph}$ with m_1^k and m_2^k being the occupation numbers of the kth-mode phonons at site 1 and site 2, respectively,

$${}_{ph}\langle\{0_1^k\},\{0_2^k\}|H_I^L|\{m_1^k\},\{m_2^k\}\rangle_{ph} = -\frac{J_\perp}{2}e^{-\frac{1}{N}\sum_k g_k^2}\left(\prod_k \frac{\left(\frac{g_k}{\sqrt{N}}\right)^{(m_1^k+m_2^k)}}{\sqrt{m_1^k!m_2^k!}}\right)(-1)^{\sum_k m_1^k}\left[b_1^\dagger b_2 + (-1)^{\sum_k (m_1^k-m_2^k)} b_2^\dagger b_1\right]. \tag{A6}$$

Using the above result and Eqs. (12) and (13) (with κ replaced by $\bar{\kappa} \equiv -\frac{J_\perp e^{-\frac{1}{N}\sum_k g_k^2}}{2}$), we calculate the four terms in the master equation (11); in the regime where $\Delta\varepsilon \gg J_\perp e^{-\frac{1}{N}\sum_k g_k^2}$, we can write the differential equation for $\langle 10|\tilde{\rho}_s(t)|01\rangle$ to be

$$\begin{aligned}\frac{d\langle 10|\tilde{\rho}_s(t)|01\rangle}{dt} = -i\bar{\kappa}^2 {\sum_{\{n_1^k\},\{n_2^k\}}}' \bar{C}_n\Bigg[\langle 10|\tilde{\rho}_s(t)|01\rangle\left(\frac{e^{-i(\bar{\omega}_n-\Delta\varepsilon)t}}{\bar{\omega}_n-\Delta\varepsilon} - \frac{e^{i(\bar{\omega}_n+\Delta\varepsilon)t}}{\bar{\omega}_n+\Delta\varepsilon} - \frac{2\Delta\varepsilon}{\bar{\omega}_n^2-\Delta\varepsilon^2}\right)\\ + \langle 01|\tilde{\rho}_s(t)|10\rangle(-1)^{\sum_k(n_1^k-n_2^k)}e^{2i\Delta\varepsilon t}\left(\frac{e^{i(\bar{\omega}_n-\Delta\varepsilon)t}}{\bar{\omega}_n-\Delta\varepsilon} - \frac{e^{-i(\bar{\omega}_n+\Delta\varepsilon)t}}{\bar{\omega}_n+\Delta\varepsilon} - \frac{2\Delta\varepsilon}{\bar{\omega}_n^2-\Delta\varepsilon^2}\right)\Bigg].\end{aligned} \tag{A7}$$

The corresponding complex-conjugate equation would describe the dynamics for $\langle 01|\tilde{\rho}_s(t)|10\rangle$. Here, we have defined $\bar{\omega}_n \equiv \sum_k \omega_k(n_1^k+n_2^k)$, $\bar{C}_n \equiv \prod_k \frac{(\frac{g_k}{\sqrt{N}})^{2(n_1^k+n_2^k)}}{n_1^k!n_2^k!}$, $T \equiv t-\tau$, and $\sum'_{\{n_1^k\},\{n_2^k\}}$ as the sum over all combinations of $\{n_1^k\}$ and $\{n_2^k\}$ excluding the case when $\{n_1^k\}=\{0_1^k\}$ and $\{n_2^k\}=\{0_2^k\}$. Similarly, one can obtain the following differential equation for $\langle 10|\tilde{\rho}_s(t)|10\rangle$:

$$\frac{d\langle 10|\tilde{\rho}_s(t)|10\rangle}{dt} = -2\bar{\kappa}^2 {\sum_{\{n_1^k\},\{n_2^k\}}}' \bar{C}_n\left[\langle 10|\tilde{\rho}_s(t)|10\rangle\left(\frac{\sin(\bar{\omega}_n+\Delta\varepsilon)t}{\bar{\omega}_n+\Delta\varepsilon} + \frac{\sin(\bar{\omega}_n-\Delta\varepsilon)t}{\bar{\omega}_n-\Delta\varepsilon}\right) - \frac{\sin(\bar{\omega}_n+\Delta\varepsilon)t}{\bar{\omega}_n+\Delta\varepsilon}\right]. \tag{A8}$$

Now, to get a closed form of Eqs. (A7) and (A8), we write

$${\sum_{\{n_1^k\},\{n_2^k\}}}' \bar{C}_n e^{\pm i\bar{\omega}_n T} = \prod_k\left(\sum_{n_1^k}\frac{\left(\frac{g_k^2}{N}\right)^{n_1^k}}{n_1^k!}e^{\pm i\omega_k n_1^k T}\sum_{n_2^k}\frac{\left(\frac{g_k^2}{N}\right)^{n_2^k}}{n_2^k!}e^{\pm i\omega_k n_2^k T}\right) - 1 = \exp\left[\frac{2}{N\pi}\int_0^\infty d\omega\frac{J(\omega)}{\omega^2}e^{\pm i\omega T}\right] - 1, \tag{A9}$$

where the spectral function of the phonon bath $J(\omega) = \pi\sum_k g_k^2\omega_k^2\delta(\omega-\omega_k)$ characterizes the HCB-phonon coupling for different phonon-frequency modes. Using the above expression, we can write the differential equations (A7) and (A8) as

$$\begin{aligned}\frac{d\langle 10|\tilde{\rho}_s(t)|01\rangle}{dt} = -2\bar{\kappa}^2\int_0^t d\tau\Bigg\{\langle 10|\tilde{\rho}_s(t)|01\rangle e^{i\Delta\varepsilon T}\left[\exp\left(\frac{2}{N\pi}\int_0^\infty d\omega\frac{J(\omega)}{\omega^2}\cos(\omega T)\right)\cos\left(\frac{2}{N\pi}\int_0^\infty d\omega\frac{J(\omega)}{\omega^2}\sin(\omega T)\right) - 1\right]\\ - \langle 01|\tilde{\rho}_s(t)|10\rangle e^{i\Delta\varepsilon(t+\tau)}\left[\exp\left(-\frac{2}{N\pi}\int_0^\infty d\omega\frac{J(\omega)}{\omega^2}\cos(\omega T)\right)\cos\left(\frac{2}{N\pi}\int_0^\infty d\omega\frac{J(\omega)}{\omega^2}\sin(\omega T)\right) - 1\right]\Bigg\}\end{aligned} \tag{A10}$$

and

$$\begin{aligned}&\frac{d\langle 10|\tilde{\rho}_s(t)|10\rangle}{dt}\\ &= -2\bar{\kappa}^2\int_0^t d\tau\Bigg\{2\langle 10|\tilde{\rho}_s(t)|10\rangle\cos(\Delta\varepsilon T)\left[\exp\left(\frac{2}{N\pi}\int_0^\infty d\omega\frac{J(\omega)}{\omega^2}\cos(\omega T)\right)\cos\left(\frac{2}{N\pi}\int_0^\infty d\omega\frac{J(\omega)}{\omega^2}\sin(\omega T)\right) - 1\right]\\ &- \left[\exp\left(\frac{2}{N\pi}\int_0^\infty d\omega\frac{J(\omega)}{\omega^2}\cos(\omega T)\right)\cos\left(\Delta\varepsilon T + \frac{2}{N\pi}\int_0^\infty d\omega\frac{J(\omega)}{\omega^2}\sin(\omega T)\right) - \cos(\Delta\varepsilon T)\right]\Bigg\}.\end{aligned} \tag{A11}$$

The first-order nonhomogeneous differential Eq. (A11) can be solved analytically.

In principle, $J(\omega)$ can assume a variety of forms based on the nature of the phonon bath; however, for simplicity, we use a continuous uniform distribution of phonon frequencies within a small frequency window characterized by an upper cutoff ω_u and a lower cutoff ω_l. The density of states for Einstein phonons is described by $D(\omega_k) = N\delta(\omega_k-\omega_0)$ where ω_0 is a fixed

frequency. Moreover, we consider a weak k dependence of the coupling strength g_k and write

$$D(\omega_k)g_k^2 = N\delta(\omega_k - \omega_0)g^2. \tag{A12}$$

Here, we should mention that in systems such as the manganites (where the carriers are coupled predominantly only to optical phonons), the weak k dependence of g_k is quite valid. Following Eq. (A12), we make a simple generalization of the Einstein model and replace the Dirac delta function by a box function of width $(\omega_u - \omega_l)$ and height $\frac{1}{(\omega_u - \omega_l)}$:

$$D(\omega_k)g_k^2 = g^2 \frac{N}{\omega_u - \omega_l}\Theta(\omega_k - \omega_l)\Theta(\omega_u - \omega_k), \tag{A13}$$

where $\Theta(\omega)$ is the unit step function. With the above form for the density of states, we calculate the following:

$$\frac{1}{N\pi}\int_0^\infty \frac{J(\omega)}{\omega^2}d\omega = \frac{1}{N}\int_0^\infty d\omega_k D(\omega_k)g_k^2 = g^2, \tag{A14}$$

$$\frac{1}{N\pi}\int_0^\infty \frac{J(\omega)}{\omega^2}\cos\omega T\, d\omega = \frac{1}{N}\int_0^\infty d\omega_k D(\omega_k)g_k^2\cos\omega_k T = \frac{2g^2}{(\omega_u - \omega_l)T}\cos\left[\frac{(\omega_u + \omega_l)T}{2}\right]\sin\left[\frac{(\omega_u - \omega_l)T}{2}\right], \tag{A15}$$

and

$$\frac{1}{N\pi}\int_0^\infty \frac{J(\omega)}{\omega^2}\sin\omega T\, d\omega = \frac{1}{N}\int_0^\infty d\omega_k D(\omega_k)g_k^2\sin\omega_k T = \frac{2g^2}{(\omega_u - \omega_l)T}\sin\left[\frac{(\omega_u + \omega_l)T}{2}\right]\sin\left[\frac{(\omega_u - \omega_l)T}{2}\right]. \tag{A16}$$

Using the above integrals, we solve the differential Eq. (A10) numerically and plot the coherence factor C(t) in Fig. 10. Here, unlike the single-mode case, we have a continuum of phonon frequencies due to which the various harmonics in Eq. (A7) do not all rephase at the same time

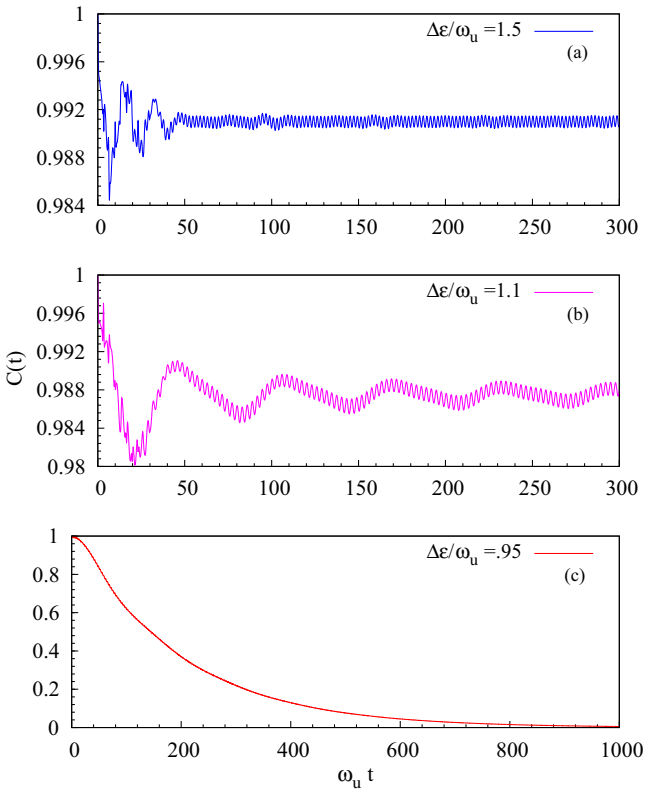

FIG. 10. (Color online) Time dependence of C(t) for $\frac{J_\perp}{\omega_u} = 0.5$, $\frac{\omega_l}{\omega_u} = 0.9$, $g = 2.0$, and different values of $\frac{\Delta\varepsilon}{\omega_u}$ leading to different scenarios.

leading to destructive interference, i.e., an irreversible decay of C(t). It is of interest to note that the structures of Eqs. (15) and (A7) are very similar; hence, the explanations that were offered in the single-mode case, for the period and amplitude of oscillations of C(t), hold also for the multimode case. For the circumstance in Fig. 10(b), the contribution from the phonon state ω_u dominates because it is the frequency that is closest to $\Delta\varepsilon$ and $\Delta\varepsilon - \omega_u$ ($\ll\omega_u$) is comparable to the width of the allowed-frequency window $\omega_u - \omega_l$. Then, the period of oscillation in Eq. (A7) can be obtained approximately from the case $|(\bar{\omega}_n - \Delta\varepsilon)t| = |(\omega_u - \Delta\varepsilon)t| = 0.1\omega_u t$; thus, the period is approximately $20\pi/\omega_u$. Furthermore, since $\Delta\varepsilon$ is close to $\bar{\omega}_n$, only a few frequencies contribute to the destructive interference leading to a gradual decay of the amplitude of oscillation in Fig. 10(b). For the situation where $\Delta\varepsilon$ equals any of the phonon eigenenergies $\bar{\omega}_n$ [such as in Fig. 10(c)], there is a complete decay of coherence due to resonance. When $\Delta\varepsilon$ is away from $\bar{\omega}_n$ [which is the case in Fig. 10(a)], there are a number of dominant phonon states having comparable contributions and these states interfere destructively, resulting in a quick decay of amplitude. Next, we study the population P(t) of the excited state $|10\rangle$ and depict its variation in Fig. 11. When the excited state is initially largely populated [such as in Fig. 11 where $\langle 10|\rho_s(0)|10\rangle = 0.8$], the behavior of P($t$) is mainly dictated by the homogeneous part of the solution obtained from Eq. (A8). Since the structures of Eqs. (16) and (A8) are very similar, we expect that the single-mode and multimode cases will have similar justifications for the period and amplitude of oscillations of P(t). The cases of $\Delta\varepsilon$ considered in Fig. 11 are the same as those studied in Fig. 10; furthermore, the same explanations hold for the period and decay of oscillations in these two figures.

Lastly, we elucidate through Fig. 12 the multimode cases [of $\Delta\varepsilon$ being an integer multiple of $\omega_{\rm avg} \equiv \frac{1}{N}\sum_k \omega_k = (\omega_u + \omega_l)/2$] when the coherence C(t) and the excited-state population P(t) undergo complete decay. Similar to the single-mode case [depicted in Figs. 2(c) and 4(c)], here too the

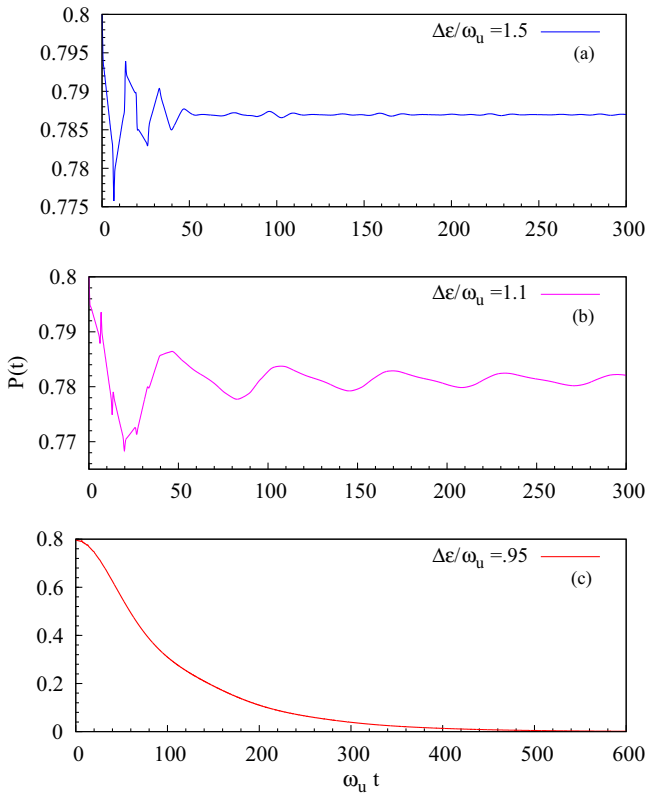

FIG. 11. (Color online) Time dependence of P(t) for $\frac{J_\perp}{\omega_u} = 0.5$, P(0) $= 0.8$, $\frac{\omega_l}{\omega_u} = 0.9$, $g = 2.0$, and different values of $\frac{\Delta\varepsilon}{\omega_u}$.

maximum decay of both C(t) and P(t) occurs when $\Delta\varepsilon$ is equal to twice the polaron energy $\frac{1}{N}\sum_k g_k^2\omega_k$ (i.e., $2g^2\omega_{\rm avg}$ for our density of states).

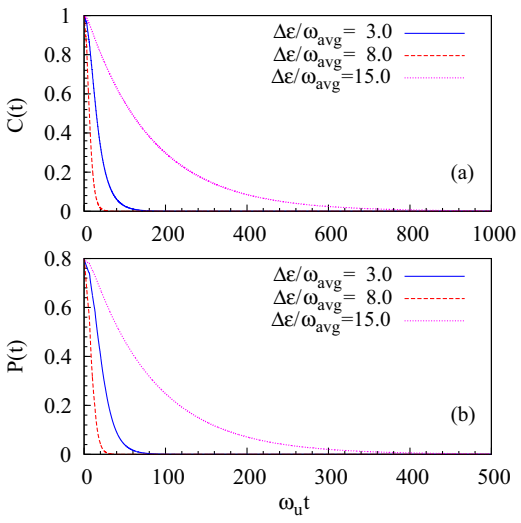

FIG. 12. (Color online) Depiction of complete decay of (a) C(t) and (b) P(t) [with P(0) $= 0.8$] at different integer values of $\frac{\Delta\varepsilon}{\omega_{\rm avg}}$ when $\frac{J_\perp}{\omega_u} = 0.5$ and $g = 2.0$. The maximum decay occurs when $\Delta\varepsilon = 2g^2\omega_{\rm avg}$.

APPENDIX B

We will begin the small-parameter analysis, for a two-site system, by first analyzing the case of zero detuning (i.e., $\Delta\varepsilon = 0$); this is to build a foundation for understanding the more complicated situation pertaining to nonvanishing $\Delta\varepsilon$ being comparable to the phonon eigenenergies ω_n. For $\Delta\varepsilon = 0$, as pointed out in Ref. [5], second-order perturbation contribution for a two-site system is given by the following [obtained by taking $N = 2$ in Eq. (26) of the main text]:

$$H^{(2)} = -\sum_m \frac{{}_{ph}\langle 0|H_I|m\rangle_{ph}\ {}_{ph}\langle m|H_I|0\rangle_{ph}}{\omega_m}$$
$$= -\frac{1}{2}J_\parallel^{(2)}\{n_1(1-n_2)+n_2(1-n_1)\}, \qquad \text{(B1)}$$

where

$$J_\parallel^{(2)} \equiv \frac{\kappa^2}{\omega}\sum_{n_1,n_2}{}' \frac{C_n}{(n_1+n_2)}$$
$$= [2f_1(g)+f_2(g)]\frac{J_\perp^2 e^{-2g^2}}{2\omega} \sim \frac{J_\perp^2}{4g^2\omega}, \qquad \text{(B2)}$$

with $C_n \equiv \frac{g^{2(n_1+n_2)}}{n_1!n_2!}$, $f_1(g) \equiv \sum_{l=1}^\infty g^{2l}/(l!l!)$, and $f_2(g) \equiv \sum_{j=1}^\infty\sum_{l=1}^\infty g^{2(j+l)}/[j!l!(j+l)]$. Then, the square of the small parameter γ is given by the ratio of the second-order perturbation $J_\parallel^{(2)}/2$ and the phonon frequency ω in H_0; i.e.,

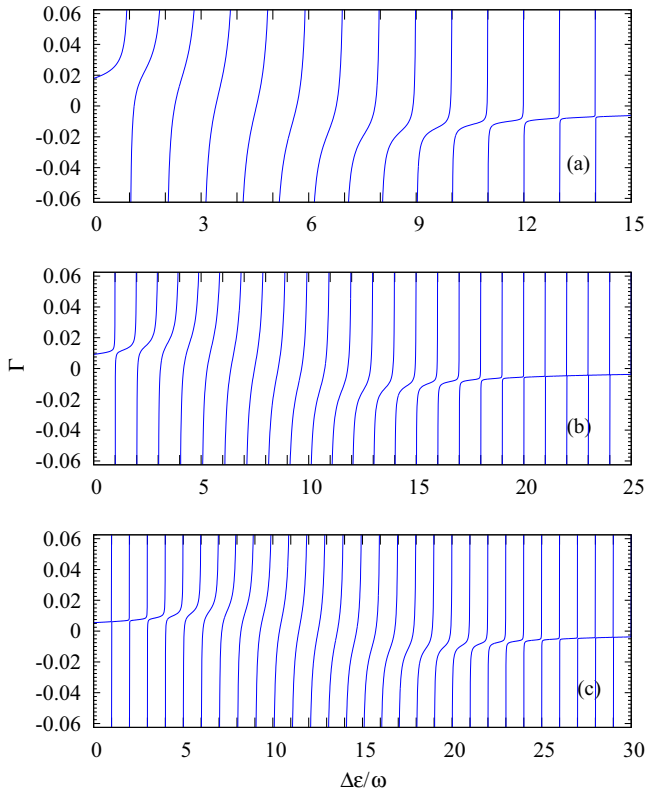

FIG. 13. (Color online) Γ is plotted with varying $\Delta\varepsilon/\omega$ for $\frac{J_\perp}{\omega} = 0.5$ when (a) $g = 1.5$, (b) $g = 2.0$, and (c) $g = 2.5$; square of small parameter $\gamma^2 = |\Gamma|$.

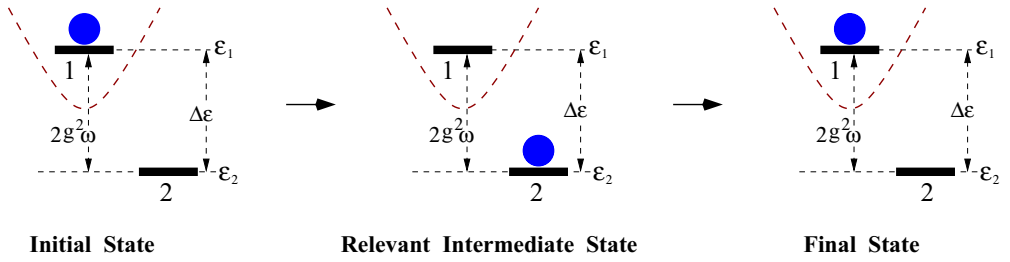

FIG. 14. (Color online) Schematic representation of the site energies and hopping process leading to minimum coherence C(t) and maximum decay of excited state P(t); the intermediate state gives the dominant contribution. Here, location of the HCB is given by the filled circle. Parabolic curve at site 1 depicts full distortion of the lattice environment at that site with corresponding energy $-g^2\omega$ ($+g^2\omega$) if the HCB is present (absent) at that site.

$\gamma \sim J_\perp/(2g\omega)$. The above expression for $J_\parallel^{(2)}/2$ can also be deduced physically as follows (with details given in Ref. [32]). The hopping process where HCB at a site i hops to its neighboring site j and back, but with the lattice having no time to distort (relax) locally at site j (site i), yields the second-order perturbation $J_\perp^2/(4\times 2g^2\omega)$ where $2g^2\omega$ is the difference between the energies of the initial state and the intermediate state. Then, the physical estimate of the square of the small parameter (γ^2) is given by the ratio of $J_\perp^2/(8g^2\omega)$ and the phonon frequency ω; consequently, $\gamma \sim J_\perp/(2g\omega)$. Actually, in Ref. [32], the small-parameter value $J_\perp/(2g\omega)$ was deduced based on taking the ratio of the dominant terms in fourth-order perturbation and second-order perturbation. It is also interesting to note that, for $\Delta\varepsilon = 0$, the square of the small parameter can be deduced to be given by $\gamma^2 = \frac{\kappa^2}{\omega^2}\sum'_{n_1,n_2}\frac{C_n}{(n_1+n_2)}$ from the dominant amplitude of the oscillatory terms on the right-hand side of Eqs. (15) and (16) in the main text.

Based on the above results for $\Delta\varepsilon = 0$, we now infer the square of the small parameter for $\Delta\varepsilon \neq 0$ from the dominant amplitude of the oscillatory terms on the right-hand side of Eqs. (15) and (16); $\gamma^2 = |\Gamma|$ where

$$\Gamma \equiv \frac{\kappa^2}{\omega^2}\sum_{n_1,n_2}{}' \frac{C_n}{[(n_1+n_2)-\Delta\varepsilon/\omega]} = \sum_{\mathbb{N}}{}' \frac{\mathbb{C}^{\mathbb{N}}}{[\mathbb{N}-\Delta\varepsilon/\omega]}. \tag{B3}$$

The smallness of the perturbation holds true as long as γ is sufficiently small compared to 1. When $\Delta\varepsilon \neq 0$, our perturbation theory still holds except for the cases when the detuning is very close to meeting the resonance condition $\Delta\varepsilon = \omega_n$. In Fig. 13, we see that the small parameter has reasonably small values (i.e., values below 0.25) even when it is slightly away from the divergences produced by resonance. One can also see that the divergence at $\Delta\varepsilon = \omega_n = 2g^2\omega$ is the strongest as the term $\mathbb{C}^{\mathbb{N}} = \frac{\kappa^2}{\omega^2}\sum_{n_1,n_2;(n_1+n_2)=\mathbb{N}} C_n$ in the expression of γ^2 is maximum at $\mathbb{N} = 2g^2$ (see Fig. 1 in the main text). Actually, as regards the hopping process in the second-order perturbation, the time scale of hopping varies depending on the lattice distortion in the intermediate state. The quickest and the most dominant hopping process would be the case when the HCB at a fully distorted site hops to the neighboring site and comes back without any change in relaxation/distortion at either of the sites; this hopping process is schematically shown in Fig. 14. The initial state is described by the occupied site with polaronic energy (lattice distortion potential) $-g^2\omega$, whereas the intermediate state for perturbation theory corresponds to the occupied second site being without distortion and the unoccupied first site having distortion energy $+g^2\omega$ [see Fig. 14 and Fig. 2(a) in Ref. [27]]. Consequently, the corresponding denominator in Eq. (B3) is given by $(\varepsilon_1 - g^2\omega) - (\varepsilon_2 + g^2\omega) = \Delta\varepsilon - 2g^2\omega$ (which is the energy difference between the initial and the intermediate states). Other divergence points, given by $\Delta\varepsilon = \omega_n \neq 2g^2\omega$, correspond to slower hopping processes where lattice distorts/relaxes by some amount during hopping. Then, the hopping amplitudes for such cases are smaller, leading to smaller prefactors of $\frac{1}{\omega_n-\Delta\varepsilon}$ in the expression of γ^2, i.e., weaker divergences.

Now, when the time scale τ_s over which the system changes appreciably is much larger than the environmental correlation time τ_c, we have a Markov process. Thus, the Markov process corresponds to the dominant interaction energy $\frac{\kappa^2}{\omega}\sum'_{n_1,n_2}\frac{C_n}{[(n_1+n_2)-\Delta\varepsilon/\omega]}$ being much smaller than the phonon frequency ω. Consequently, we have non-Markovian dynamics when $\Delta\varepsilon$ is close to phononic eigenenergies ω_n, i.e., when the system is close to resonance situation. For $\Delta\varepsilon = 0$, at strong coupling g and for large nonadiabaticity (i.e., $\frac{J_\perp}{\omega} \ll 1$), it has been shown that the non-Markovian result approaches the Markovian result (see Sec. IX and Appendix A of Ref. [5]).

[1] M. A. Nielsen and I. Chuang, *Quantum Computation and Quantum Communication* (Cambridge University Press, Cambridge, 2000).

[2] M. Schlosshauer, Rev. Mod. Phys. **76**, 1267 (2005).

[3] W. H. Zurek, Rev. Mod. Phys. **75**, 715 (2003).

[4] For a study of coherence in semiconductor DQDs, see J. R. Petta, A. C. Johnson, J. M. Taylor, E. A. Laird, A. Yacoby, M. D. Lukin, C. M. Marcus, M. P. Hanson, and A. C. Gossard,

Science **309**, 2180 (2005); H. Bluhm, S. Foletti, I. Neder, M. Rudner, D. Mahalu, V. Umansky, and A. Yacoby, Nat. Phys. **7**, 109 (2010).

[5] A. Dey and S. Yarlagadda, Phys. Rev. B **89**, 064311 (2014).

[6] H. J. Lipkin, N. Meshkov, and A. J. Glick, Nucl. Phys. **62**, 188 (1965).

[7] J. M. Fink, R. Bianchetti, M. Baur, M. Göppl, L. Steffen, S. Filipp, P. J. Leek, A. Blais, and A. Wallraff, Phys. Rev. Lett. **103**, 083601 (2009).

[8] J. Majer, J. M. Chow, J. M. Gambetta, J. Koch, B. R. Johnson, J. A. Schreier, L. Frunzio, D. I. Schuster, A. A. Houck, A. Wallraff, A. Blais, M. H. Devoret, S. M. Girvin, and R. J. Schoelkopf, Nature (London) **449**, 443 (2007).

[9] S. Morrison and A. S. Parkins, Phys. Rev. A **77**, 043810 (2008); Phys. Rev. Lett. **100**, 040403 (2008).

[10] J. Larson, Europhys. Lett. **90**, 54001 (2010).

[11] A. Blais, J. Gambetta, A. Wallraff, D. I. Schuster, S. M. Girvin, M. H. Devoret, and R. J. Schoelkopf, Phys. Rev. A **75**, 032329 (2007).

[12] G. S. Engel, T. R. Calhoun, E. L. Read, T-K. Ahn, T. Mancal, Y-C. Cheng, R. E. Blankenship, and G. R. Fleming, Nature (London) **446**, 782 (2007).

[13] A. W. Chin, A. Datta, F. Caruso, S. F. Huelga, and M. B. Plenio, New J. Phys. **12**, 065002 (2010).

[14] Y-C. Cheng and G. R. Fleming, Annu. Rev. Phys. Chem. **60**, 241 (2009).

[15] M. Ezawa, New J. Phys. **11**, 095005 (2009); Phys. Rev. B **79**, 241407(R) (2009).

[16] S. Datta, A. Das, and S. Yarlagadda, Phys. Rev. B **71**, 235118 (2005).

[17] L.-A. Wu and D. A. Lidar, Phys. Rev. Lett. **91**, 097904 (2003).

[18] F. Dorfner, L. Vidmar, C. Brockt, E. Jeckelmann, and F. Heidrich-Meisner, Phys. Rev. B **91**, 104302 (2015).

[19] S. Sayyad and M. Eckstein, Phys. Rev. B **91**, 104301 (2015).

[20] I. G. Lang and Y. A. Firsov, Zh. Eksp. Teor. Fiz. **43**, 1843 (1962) [Sov. Phys. JETP **16**, 1301 (1963)].

[21] H. P. Beuer and F. Petruccione, *The Theory of Open Quantum Systems* (Oxford University Press, Oxford, 2002).

[22] See Supplemental Material at http://link.aps.org/supplemental/10.1103/PhysRevB.92.094302 for exact evaluation of the four matrix elements occurring in the second-order, non-Markovian, quantum-master equation.

[23] Our analysis of the case with $\Delta\varepsilon = 0$ is consistent with the findings (of nearly adiabatic evolution in a polaron band at strong coupling in the Holstein model) in L. Vidmar, J. Bonča, M. Mierzejewski, P. Prelovšek, and S. A. Trugman, Phys. Rev. B **83**, 134301 (2011).

[24] S. Reja, S. Yarlagadda, and P. B. Littlewood, Phys. Rev. B **86**, 045110 (2012).

[25] Strong coupling occurs quite commonly in transition-metal oxides such as manganites; see A. Lanzara, N. L. Saini, M. Brunelli, F. Natali, A. Bianconi, P. G. Radaelli, and S.-W. Cheong, Phys. Rev. Lett. **81**, 878 (1998); A. J. Millis, P. B. Littlewood, and B. I. Shraiman, *ibid.* **74**, 5144 (1995); and Ref. [16]. As mentioned in Ref. [5], for manganites $6 < g^2 < 10$.

[26] Nonadiabaticity occurs in systems such as C60 compounds; see L. Pietronero, S. Strassler, and C. Grimaldi, Phys. Rev. B **52**, 10516 (1995).

[27] Sahinur Reja, Sudhakar Yarlagadda, and Peter B. Littlewood, Phys. Rev. B **84**, 085127 (2011).

[28] S. Datta and S. Yarlagadda, Solid State Commun. **150**, 2040 (2010).

[29] J. R. Schrieffer and P. A. Wolff, Phys. Rev. **149**, 491 (1966).

[30] S. Bravyi, D. DiVincenzo, and D. Loss, Ann. Phys. (NY) **326**, 2793 (2011).

[31] A. Dey, M. Q. Lone, and S. Yarlagadda (unpublished).

[32] R. Pankaj and S. Yarlagadda, Phys. Rev. B **86**, 035453 (2012).

[33] For a large-N system, the largest energy contribution due to terms involving closed loops is intensive. The dominant contribution, in second- and higher-order perturbation, comes from open loops. The approximate open-loop terms in zeroth-, second-, and third-order perturbation are, respectively, $J_\perp e^{-g^2} \sum_{i,j\neq i} b_i^\dagger b_j$, $[N J_\perp^2 e^{-g^2}/(g^2\omega)] \sum_{i,j\neq i} b_i^\dagger b_j$, and $[N^2 J_\perp^3 e^{-g^2}/(g^2\omega)^2] \sum_{i,j\neq i} b_i^\dagger b_j$; then, the small parameter is $J_\perp^\star/(g^2\omega)$.

[34] R. Roth and K. Burnett, Phys. Rev. A **68**, 023604 (2003).